JOURNAL OF GEOPHYSICAL RESEARCH, VOL. 93, NO. A12, PAGES 14,699–14,718, DECEMBER 1, 1988

# VLF Wave Emissions by Pulsed and DC Electron Beams in Space 1. Spacelab 2 Observations

G. D. REEVES, P. M. BANKS, T. NEUBERT, R. I. BUSH,
P. R. WILLIAMSON, AND A. C. FRASER-SMITH

*Space Telecommunications and Radioscience Laboratory, Stanford University, Stanford, California*

D. A. GURNETT

*Department of Physics and Astronomy, University of Iowa, Iowa City*

W. J. RAITT

*Center for Atmospheric and Space Science, Utah State University, Logan*

During the Spacelab 2 space shuttle mission a 1-keV, 100-mA, square-wave-modulated, electron source (FPEG) and a plasma diagnostics subsatellite (PDP) were used to investigate the properties of radio waves generated by electron beams in space. A variety of electron beam pulsing sequences were executed to investigate specific properties of the beam-plasma-wave interaction. In addition to operations conducted with the PDP in the payload bay, several investigations were conducted with the PDP operated as a free-flying satellite at distances of several hundred meters from the orbiter. In this paper we present the results of three beam operation sequences which provide new information about the characteristics of wave generation by electron beams. Those sequences are (1) the "DC flux tube connection" sequence in which the FPEG was operated with continuous electron emission while the orbiter maneuvered to connect the PDP and the orbiter on the same magnetic field line; (2) a "Pulsed flux tube connection" sequence for which the electron beam was square-wave-modulated at 1.22 kHz; and (3) a "Prox Ops" sequence in which the FPEG was again pulsed at 1.22 kHz while the PDP was mounted in the orbiter payload bay rather than operating as a free-flying satellite. Analysis of the amplitudes of VLF emissions from these FPEG sequences allows comparison of broadband emissions from the dc and pulsed electron beams, comparison of broadband and narrow-band emissions during the pulsed electron beam emissions, and investigation of the production and propagation properties of radio waves generated by dc and pulsed electron beams in space plasmas. Spectrograms showing the general characteristics of the ambient wave environment and the wave environment generated during these three sequences are presented. The results of electron beam-generated wave observations from the STS 3/OSS 1 mission were verified. Both dc and modulated electron beams produce copious broadband emissions. Square-wave-modulated electron beams produce narrow-band radiation at the pulsing frequency and its harmonics along with the broadband emissions. The time evolution and spectral structure of broadband and narrow-band emissions are analyzed. Our observations indicated that dc, 50-mA electron beams and pulsed, 50% duty cycle, 100-mA beams produce broadband radiation which is comparable in intensity and spectral shape at all points for which the wave field was sampled. Observation of the waves produced by the electron beam during the flux tube connections indicates that there are three zones of wave emissions characterized by the amplitude of waves in those spatial regions. Zone 1 is a highly disturbed region near the beam with very intense wave activity. Zone 2 is a region of wave activity which decreases rapidly with increasing distance from the beam, and zone 3 contains lower amplitude emissions which appear to be near-field contributions. The amplitude of narrow-band emissions is in good agreement with the predictions of theory for waves generated through the Cherenkov resonance with wave normal angles less than the resonance cone angle, and the harmonic structure of the narrow-band radiation is found to be dependent on the beam propagation characteristics.

## 1. INTRODUCTION

Since the first experiment with electron beams in space plasmas [*Hess*, 1969] there has been continued and growing interest in beam-plasma experiments conducted in the ionosphere and magnetosphere. Rocket-borne electron beam experiments have been used to investigate a large range of phenomena including propagation of an electron bunch in the magnetosphere [*Winckler*, 1980], electrical charging of rockets [e.g., *Jacobsen and Maynard*, 1980; N. B. Myers et al., CHARGE 2, A sounding rocket payload to investigate vehicle charging effects due to electron beam emissions., submitted to *J. Spacecr. Rockets.*, 1988 ], electric fields at geosynchronous altitudes [*Meltzner*, 1978], radio wave emission from modulated electron beams [*Gendrin*, 1974; *Holzworth and Koons*, 1981; *Winckler et al.*, 1984, 1985], and



Paper number 88JA03596.
0148-0227/88/88JA-03596$05.00

the charging and wave generation mechanisms involved in a tethered rocket system [*Sasaki et al.*, 1986*a*].

The first electron beam experiment to be carried on the space shuttle was flown on the March 1982 flight, STS 3, as part of the vehicle charging and potential (VCAP) experiment on the Office of Space Science 1 (OSS 1) mission [*Banks et al.*, 1987]. Cooperative use of a square-wave-modulated (1-keV, 50/100-mA) fast pulsed electron generator (FPEG) and the instruments on the University of Iowa plasma diagnostics package (PDP) permitted numerous observations of the interaction of the electron beam with the ambient plasma environment in the vicinity of the orbiter. These experiments, because of the relatively long duration of the orbit, could be used to investigate the disturbed plasma environment around the orbiter [*Shawhan et al.*, 1984*a*; *Banks et al.*, 1987], charging of the orbiter during passive conditions and during electron beam injection in a variety of plasma environments [*Hawkins*, 1988], and the production of waves produced by both dc and square-wave-modulated electron beams [*Shawhan et al.*, 1984*b*; *Reeves et al.*, 1988].

Three shuttle-based electron beam experiments have followed. The Space Experiments with Particle Accelerators (SEPAC) beam-plasma experiments were flown on the Spacelab 1 mission in 1983. The SEPAC experiments utilized a higher-power electron beam than the VCAP/PDP (up to 5 keV, 300 mA), a plasma plume injector, a neutral gas plume injector, a TV camera, and a diagnostics package to investigate the properties of spacecraft charging, neutralization, and return currents for relatively high power electron beams. The SEPAC experiments and results have been reported by *Obayashi et al.* [1982], *Akai* [1984], *Sasaki* [1986*b*], *Cai et al.* [1987], and *Neubert et al.* [1986*a*]. The separate phenomena induced by charged particle beams (PICPAB) experiment investigated the radiation produced by operation of the electron beam [*Beghin et al.*, 1984].

More recent electron beam experiments in space took place on the Spacelab 2 mission in July and August 1985. Spacelab 2 included a reflight of VCAP and the PDP. During this mission the PDP was released as a free-flying satellite for a period of six hours. During the free flight the orbiter and the PDP completed six Earth orbits while the orbiter maneuvered around the PDP, allowing measurement of the plasma and wave environment out to separations of several hundred meters. Four periods of the free flight included carefully planned magnetic flux tube connections in which the orbiter maneuvered into a position such that it passed through the same geomagnetic field lines as the PDP. Two flux tube connections were used to study the effects of the passive interaction of the orbiter with the ionosphere, one flux tube connection took place with the FPEG operating in dc mode with a 50-mA current, and during the final connection the FPEG was pulsed at 1.22 kHz, 100-mA with a duty cycle of 50% (beam on-time equals beam off-time). A total of 325 electron beam pulsing sequences were conducted with the PDP free-flying and mounted in the payload bay.

An overview of the Spacelab 2 mission is forthcoming in the work by P. M. Banks et al. (Results of vehicle charging, plasma densities, and wave generation experiments on Spacelab 2, submitted to *J. Spacecr. Rockets*, 1988; hereafter P. M. Banks et al., submitted manuscript, 1988). *Gurnett et al.* [1986] and *Farrell et al.* [1988] reported on resonance cone, whistler mode radiation observed during the DC flux tube connection using filter bank data in the range 31 Hz to 17.8 MHz. Results from the PDP wideband VLF wave receiver during the Pulsed flux tube connection were reported by *Bush et al.* [1987] and *Neubert et al.* [1988].

## 2. Experiment Description

This paper presents the electron beam wave generation results from three separate pulsing sequences. These are the "DC flux tube connection," the "Pulsed flux tube connection," and the "Prox Ops" sequences. Details of the orbital and instrumental parameters for these sequences are given in Table 1. During the DC and Pulsed flux tube connections, the PDP was released as a free-flying satellite, and the orbiter maneuvered around it so that the separation of the orbiter and the PDP would allow the sampling wave fields in a range of positions with respect to the beam.

Figure 1 shows the trajectory of the PDP relative to the orbiter. The start and stop times for each sequence are noted, and one point is plotted every 30 s. The coordinate system is picked with the orbiter at the origin. The vertical axis is the distance parallel to the magnetic field line which passes through the orbiter, hereafter referred to as the "conjunction field line," and the horizontal axis is the distance perpendicular to that field line. (Note that the conjunction field line refers to the instantaneous field line connected to the orbiter, not a geomagnetic field line which is fixed in space.) Negative distances on the horizontal axis correspond to times when the PDP was approaching the conjunction field line, and positive distances correspond to times when the PDP was receding. For $r_\perp = 0$, the PDP and the orbiter lie on the same geomagnetic field line, and this is referred to as the flux tube connection. The attitude of the orbiter was such that at all times the orbiter $z$ axis (rising out of the payload bay, perpendicular to the plane containing the wings) pointed toward the PDP. Beam electrons follow a helical trajectory along the field line, so the angle between the conjunction field line and a line connecting the orbiter to the PDP defines the pitch angle of the electron beam as well as the ray angles of wave emissions detected by the PDP. During the Prox Ops sequence the PDP was mounted in the payload bay 6.62 m from the FPEG aperture (Figure 2) and the FPEG was operated in the same mode as during the Pulsed flux tube connection.

The data presented in this paper were acquired using the wideband receiver on the University of Iowa plasma diagnostics package. A description of the use of the wideband receiver for making VLF wave observations can be found in the work by *Reeves et al.* [1988] and is summarized here. The wideband receiver measured two frequency bands, ELF and VLF, with frequency limits 40–1000 Hz and 0.4–10 kHz respectively. Data in the two bands were obtained simultaneously. The wideband receiver was connected alternately to a 3.89-m electric dipole antenna and a 16-inch-long, 10,000-turn magnetic field search coil. Every fourth magnetic antenna period was replaced by an antenna period when the wave receiver was connected to a Langmuir probe, and during those times the broadband wave data cannot be used. In addition to this antenna switching pattern, the VLF band could measure signals heterodyned from higher frequency ranges into the 0–10 kHz frequency range. The VLF band monitored the approximate frequency ranges 0–10 kHz for 26 s, 20–10 kHz (with inverted frequency response) for 13 s,

TABLE 1. Instrumental and Orbital Parameters for the Spacelab 2 Mission Which Are Relevant to the DC and Pulsed Flux Tube Connections and the Prox Ops Sequence

| Instrumental or Orbital Parameters | DC Flux Tube Connection | Pulsed Flux Tube Connection | Prox Ops Sequence |
|---|---|---|---|
| beam energy, keV | 1 | 1 | 1 |
| beam current, mA | 50 | 100 | 100 |
| duty cycle, % | 100 | 50 | 50 |
| location of PDP | free flight | free flight | payload bay 6.62 m from FPEG |
| sequence start time, day/UT | 213/0328 | 213/0404 | 212/1831 |
| sequence stop time, day/UT | 213/0339 | 213/0417 | 212/1839 |
| FPEG turn-on, day/UT | 213/0330:12 | 213/0411:13 | 212/1831:42 |
| FPEG turn-off, day/UT | 213/0337:22 | 213/0418:23 | 212/1838:52 |
| altitude of the orbiter, km | 325 | 321 | 327 |
| start latitude | 28° | 3° | 48° |
| stop latitude | 54° | −38° | 48° |
| start longitude | 15° | 1° | 14° |
| stop longitude | 18° | 4° | 27° |
| day/night | day | night | day |
| measured electron density, $cm^{-3}$ | $1 \times 10^5$ | $3 \times 10^4$ | unavailable |
| IRI predicted electron density, $cm^{-3}$ | $3.5 \times 10^5$ | $8.1 \times 10^4$ | $6.5 \times 10^5$ |
| magnetic field strength, G * | .407 | .225 | .476 |
| magnetic field azimuth, * | 356° | 14° | 99° |
| magnetic field elevation, * | ≈ 0° | ≈ 0° | 115° |
| shuttle velocity, km/s | 7.7 | 7.7 | 7.7 |
| velocity azimuth, * | 354° | 166° | 354° |
| velocity elevation, * | 75° | 126° | 118° |
| $f_{pe}$, † MHz | 2.8 | 1.6 | 4.0 |
| $f_{ce}$, MHz | 1.1 | .63 | 1.3 |
| $f_{ci}(O^+)$, Hz | 38.8 | 21.5 | 45.4 |
| $f_{ci}(H^+)$, Hz | 611 | 344 | 727 |
| $f_{LHR}$, † kHz | 6.6 | 3.6 | 8.4 |

Orbital parameters are from the best estimated trajectory tables for Spacelab 2.
Characteristic frequencies are calculated for the measured or estimated magnetic field strengths and electron densities. For the Prox Ops sequence, the electron density was taken to be one third of that predicted by the international reference ionosphere (IRI) model [*Bilitza*,1986] based on comparison of measured and predicted densities for the other two sequences.
* Values are for the time of closest approach to the conjunction field line.
† Calculated using 2% $H^+$ and measured electron densities for the DC and Pulsed flux tube connections and $n_e = \frac{1}{3}6.5 \times 10^5$ $cm^{-3}$ for the Prox Ops sequence.

and 20–30 kHz for 13 s. The antenna switching pattern is illustrated in Figure 3. The antenna switching pattern is the origin of many of the apparent gaps or discontinuities in the wave data as well as the lack of simultaneous electric and magnetic field data.

In addition to the wideband wave receiver, the PDP contained a Langmuir probe which was used to measure the plasma electron density, a low-energy proton and electron differential energy analyzer (LEPEDEA) which measured electron and proton energy spectra, a triaxial flux gate magnetometer which measured the magnitude and direction of the ambient magnetic field, the IMP/Helios filter bank, and a variety of other instruments which were not used in this experiment *[Shawhan et al., 1984a]*. The IMP/Helios instrument consisted of 16, 10% bandwidth filters in the range 31 Hz to 17.8 MHz which were connected to the electric dipole and magnetic search coil antennas to provide additional wave field information. The vehicle charging and potential (VCAP) experiment package contained the FPEG, a Langmuir probe, a spherical retarding and potential analyzer and charge and current probes. These instruments provided information on vehicle charging and return current collection during ambient conditions and during electron beam injection [*Banks et al.*, 1987].

## 3. OBSERVATIONS

The wideband wave receiver data are in the form of an analog broadband audio waveform. The amplitude of the signal is kept within strict limits with an automatic gain control (AGC) with a 100-dB dynamic range. In order to

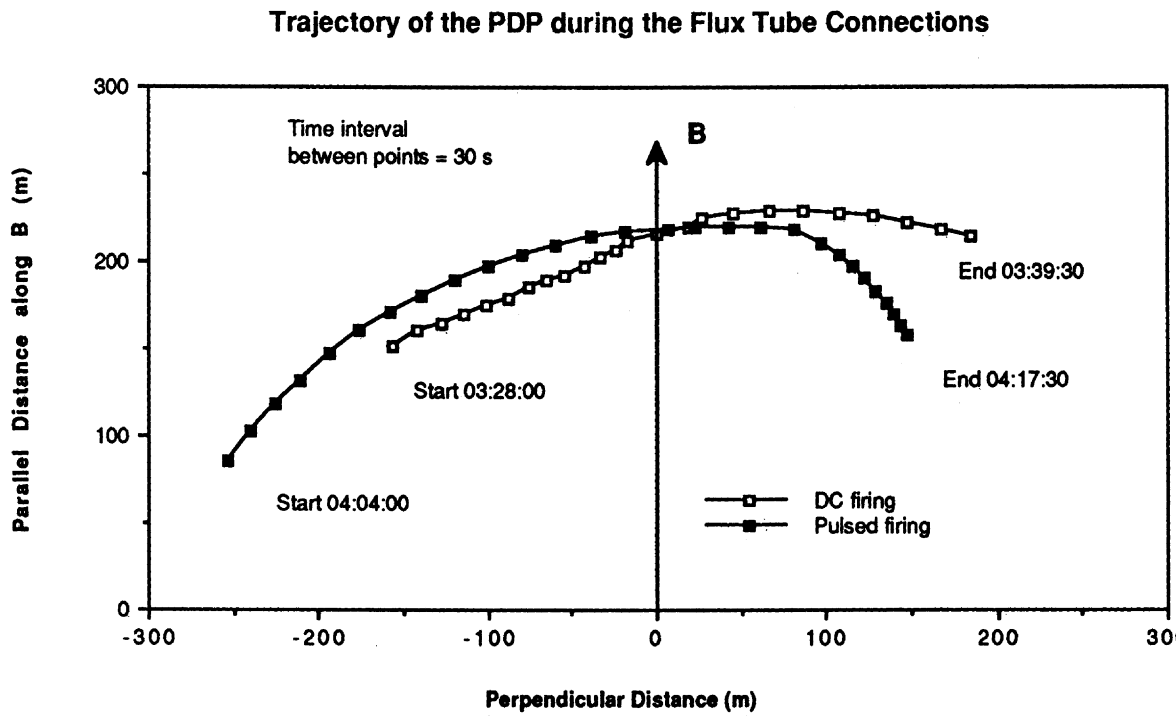


Fig. 1. The trajectory of the PDP for two flux tube connections. The orbiter is at the origin, and parallel and perpendicular refer to the conjunction field line connected to the orbiter. The trajectories for the DC and the Pulsed flux tube connections are shown. Sequence start and stop times are noted, and one point is plotted for every 30 s.

analyze the amplitude of the spectral components of the received wave signal, select periods of VLF band wave data were digitized at a rate of 25,000 samples/s which, in conjunction with the band pass of the receiver, leaves the frequency ranges of interest without aliased signals. These data were then Fourier transformed into time-frequency spectrograms with a resolution of 12.207 Hz and 40.96 ms. At this point the spectrograms can be displayed to observe the general wave characteristics, but the AGC modulation of the signal is still superimposed on the data (see, for example, Plate 1 of this paper and Figures 2 and 3 of *Bush et al.* [1987]). In the following subsection we present spectrograms from the three sequences under consideration and discuss the general observations.

*General Results*

Plate 1 shows four spectrograms produced from the VLF wideband electric antenna data. (Plate 1 is shown here in black and white. The color version can be found in the separate color section of this issue.) In each spectrogram one antenna period is shown. The antenna switching pattern is most obvious in Plates 1*c* and 1*d*. We note again that the first 26 s are 0–10 kHz, the next 13 s are 10–20 kHz and are inverted (with 10 kHz at the top of the scale), and the final 13 s are 20–30 kHz. The AGC modulation of the signal keeps the total wave amplitude in the band roughly constant, and therefore the amplitudes are relative.

*The ambient wave environment.* Plate 1*a* is the electric response during the Pulsed flux tube connection before the FPEG is turned on. At this time the PDP is located at a position with respect to the orbiter which is 100 m along the conjunction field line and 250 m perpendicular to it (-250 m in Figure 1). The electric field is seen to be very highly time varying with the strongest wave response occurring due to natural atmospherics, including whistlers, and to wave emissions due to orbiter thruster operation. (orbiter thruster firings are frequent during the flux tube connections.) During this antenna period the wave spectrum is dominated by small-dispersion atmospherics. The whistlers can be identified in the spectrograms by a slight "hook" in the frequency response at low frequencies. They were found to have amplitudes of up to $5 \times 10^{-5}$ V/m as measured with the electric dipole antenna and $10^{-5}$ nT as measured with the magnetic search coil antenna during daytime conditions. During nighttime conditions, the maximum amplitudes were $10^{-7}$ V/m and $10^{-6}$ nT. The amplitudes of the whistler signals observed in Plate 1*a* peak between 3–4 kHz, which is in the range of the lower hybrid frequency, which was approximately 3.6 kHz at this time. The maximum amplitude of whistlers reported by *Hayakawa et al.* [1986] during daytime conditions was $6 \times 10^{-4}$ V/m at $25^0$ latitude and $2.5 \times 10^{-4}$ V/m at $35^0$ latitude. It has also been reported in the literature [*Helliwell*, 1965] that whistlers are often observed to have enhanced amplitudes near the lower hybrid frequency, so we find that our measurements are in general agreement with previous observations.

The effect of the orbiter reaction control system (RCS) and attitude control system (ACS) on the plasma wave response was usually to enhance plasma wave amplitudes by up to an order of magnitude above existing levels. The effects of thrusters upon the VLF wave signals and return current distribution during electron beam operation are active areas of investigation and will be reported elsewhere.

Another feature observed in the ambient wave spectrum during the flux tube connections is the presence of variable

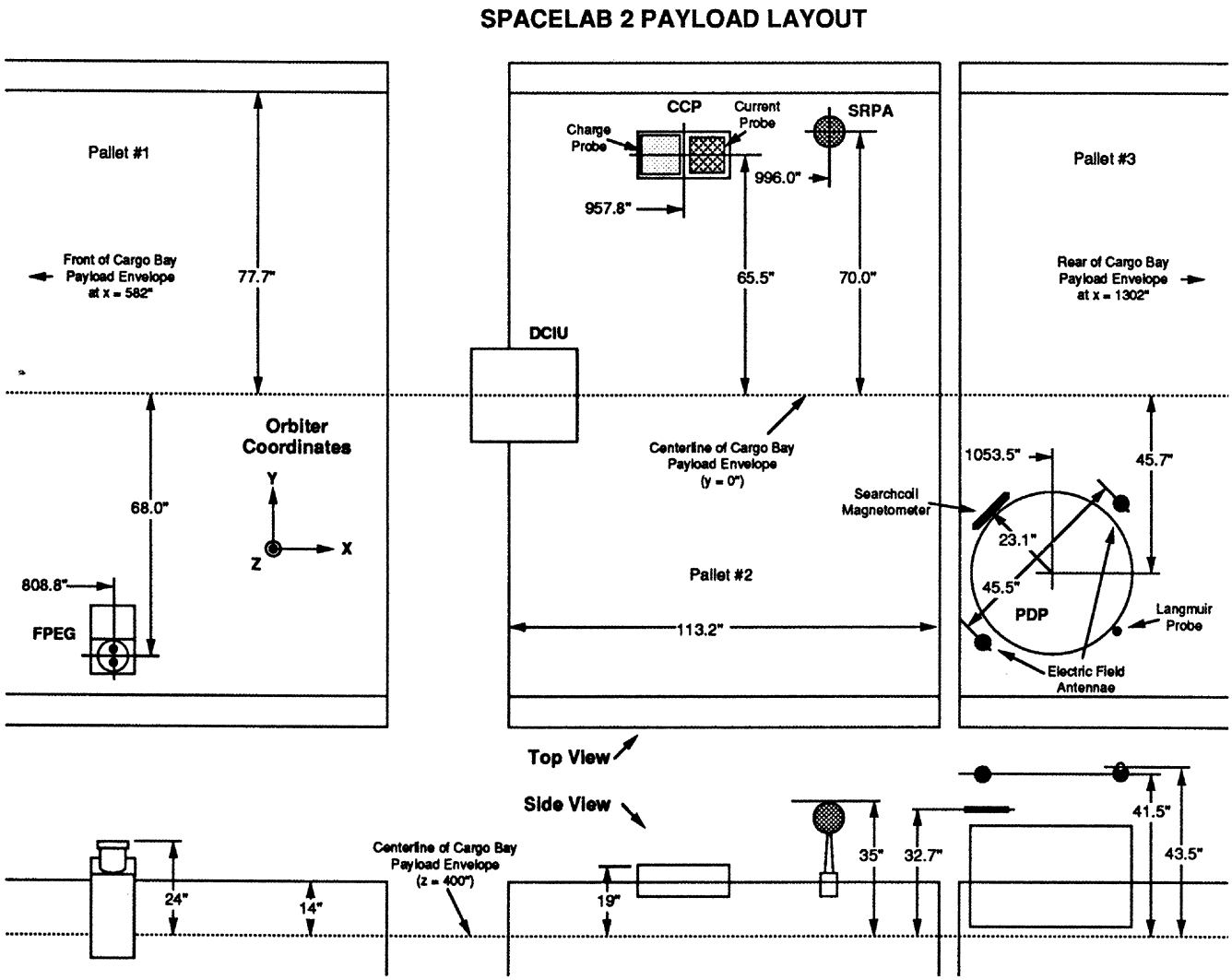


Fig. 2. The position of the FPEG, the PDP, the charge and current probes (CCP), and other instruments mounted in the payload bay on Spacelab 2. The orbiter coordinate system is also indicated in the figure.

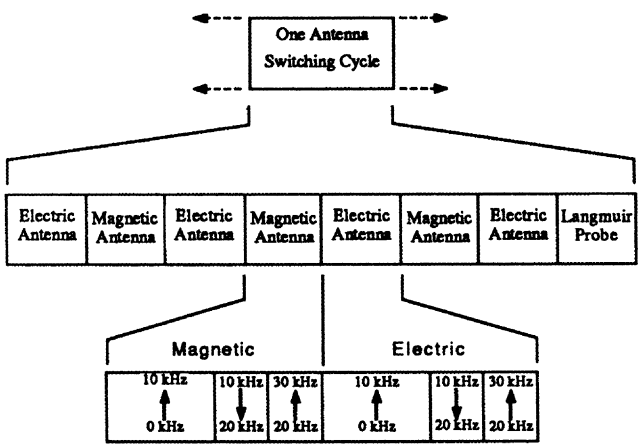


Fig. 3. The antenna switching pattern. One antenna switching cycle consists of eight "antenna periods" which alternate between electric and magnetic antennas with the final magnetic antenna period being replaced by a Langmuir probe period. Both the ELF and VLF bands are subject to the same, synchronized, switching pattern. In addition, the VLF band is subjected to a frequency switching pattern. In both the electric and magnetic antenna periods, 0–10 kHz is measured for half a period, and 20–10 kHz (inverted) and 20–30 kHz are measured for a quarter period.

frequency, narrow-band emissions between 7 and 16 kHz with amplitudes which can exceed $10^{-6}$ V/m. The frequency of the narrow-band emissions varies with time and appears to repeat with a period of $\sim$ 13 s. During the free flight, the PDP was spin stabilized and rotated with a period of $\sim$ 13 s. It is curious that the variation of these narrow-band signals appears with the spin period of the PDP rather than with half the spin period as would be expected for a symmetric single-axis antenna. Although the whistlers are observed with both the electric and the magnetic antennas, these narrow-band emissions are observed only through their electric field signature. Waves with similar features have been observed from rockets and satellites. They are thought to be generated by the interaction of the spacecraft with the ambient plasma as discussed by *Neubert et al.* [1986*b*] and references therein.

*The DC flux tube connection.* Plate 1*b* shows the electric field response during the DC flux tube connection when the FPEG is firing and the PDP is near the conjunction field line. During this antenna period the PDP is located 225 m along and 45 m perpendicular to the conjunction field line. It is apparent that operation of the FPEG produces broad-band emissions at all frequencies within the limits of the

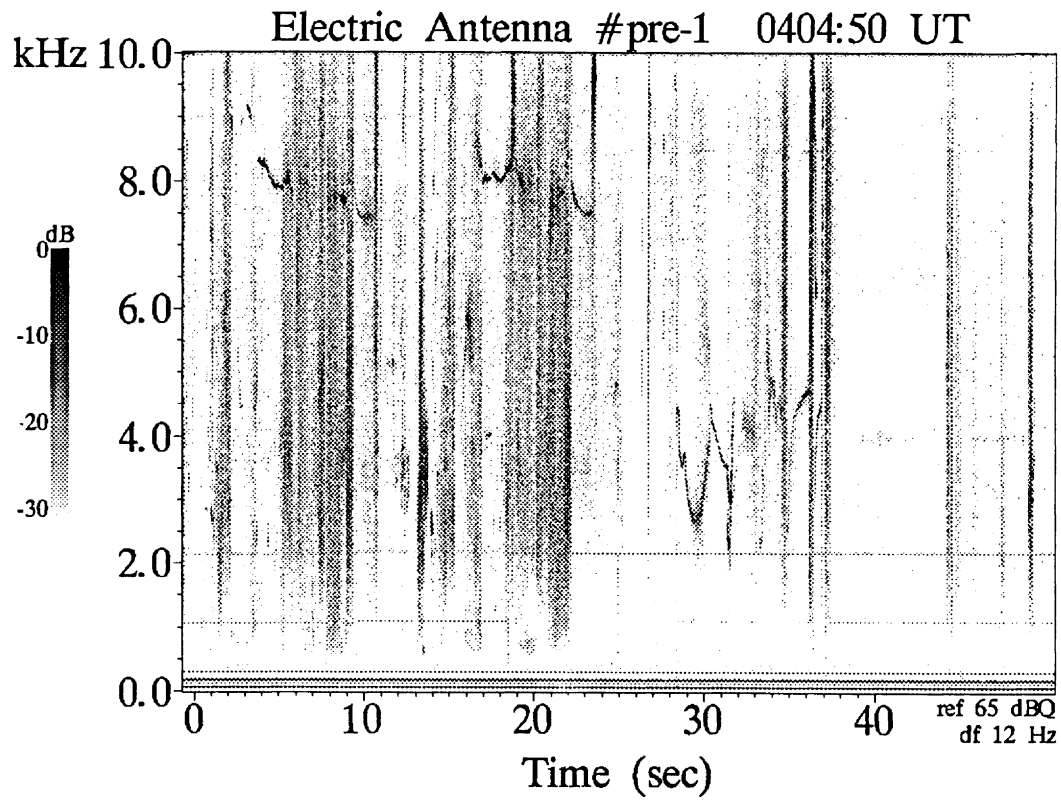


Plate 1*a*. A spectrogram showing the wave response during ambient conditions with no FPEG operations.

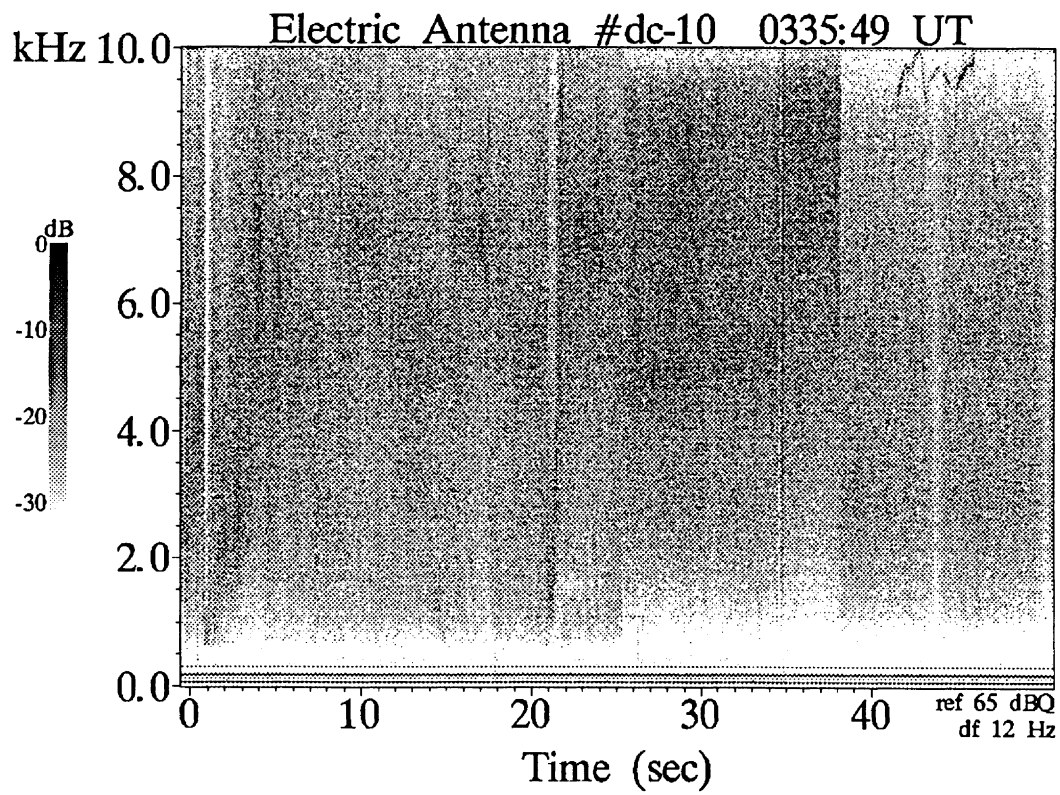


Plate 1*b*. A spectrogram showing the wave response during the DC flux tube connection sequence.

Plate 1. Spectrograms of four antenna periods during the Spacelab 2 mission. The color version and a complete description of this figure can be found in the separate color section in this issue.

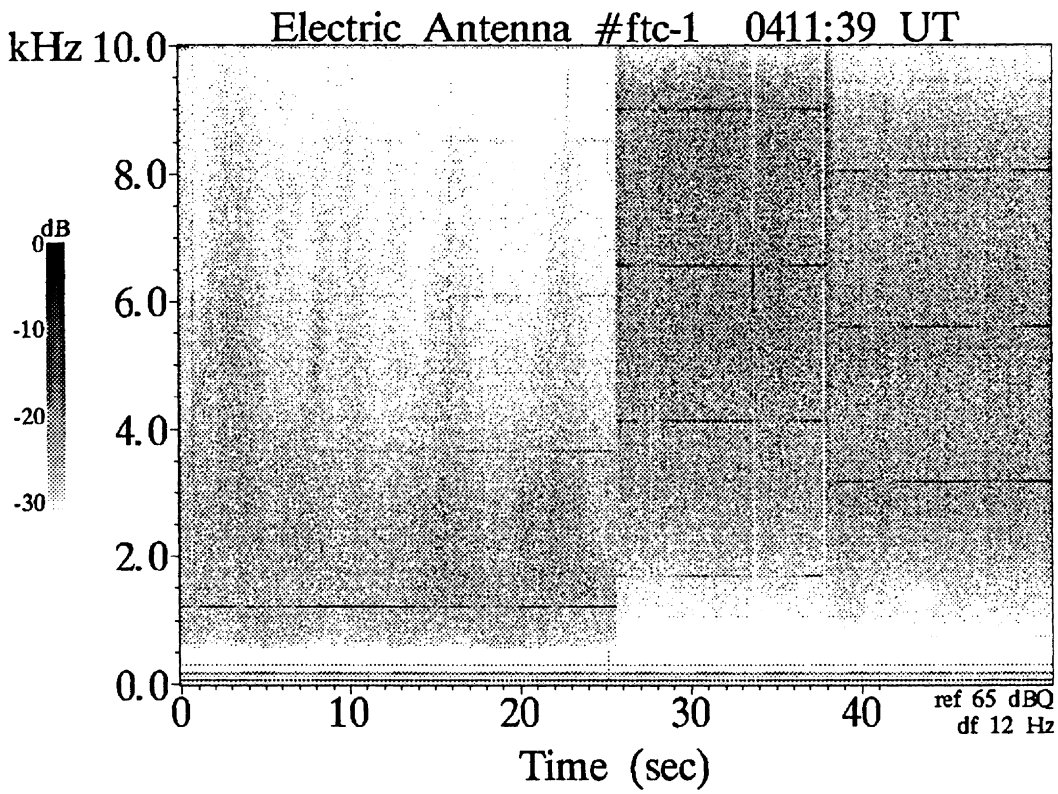


Plate 1*c* A spectrogram showing the wave response during the Pulsed flux tube connection sequence.

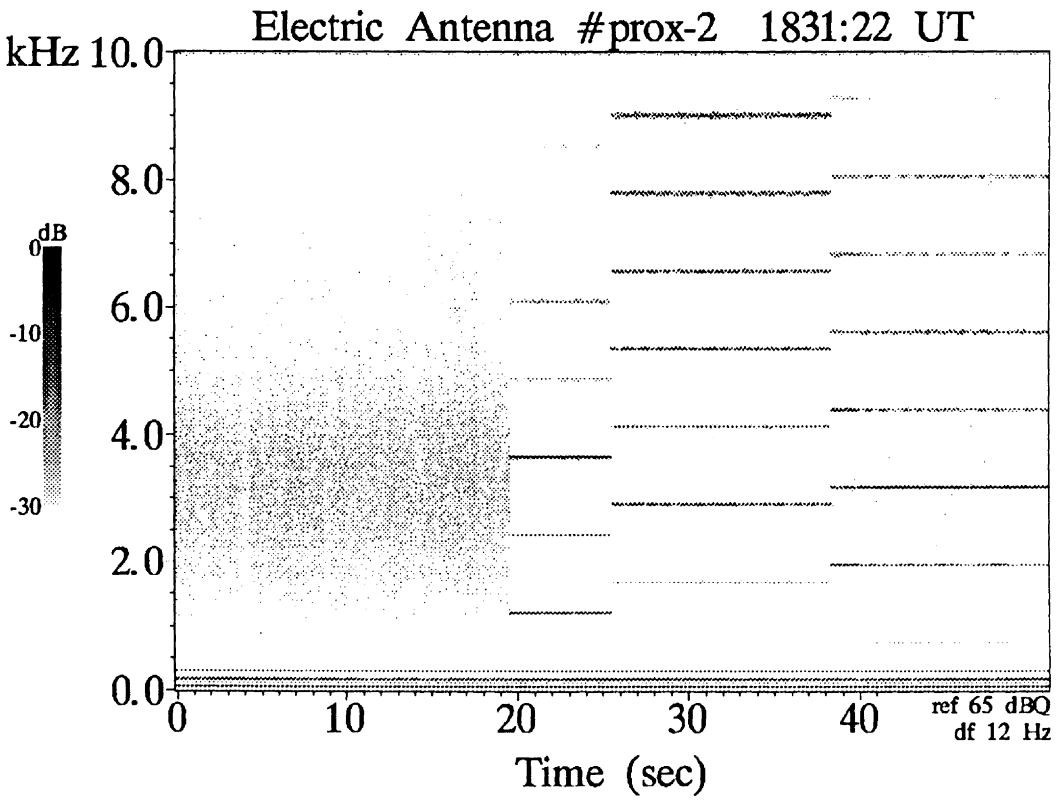


Plate 1*d* A spectrogram showing the wave response during the Prox Ops sequence.

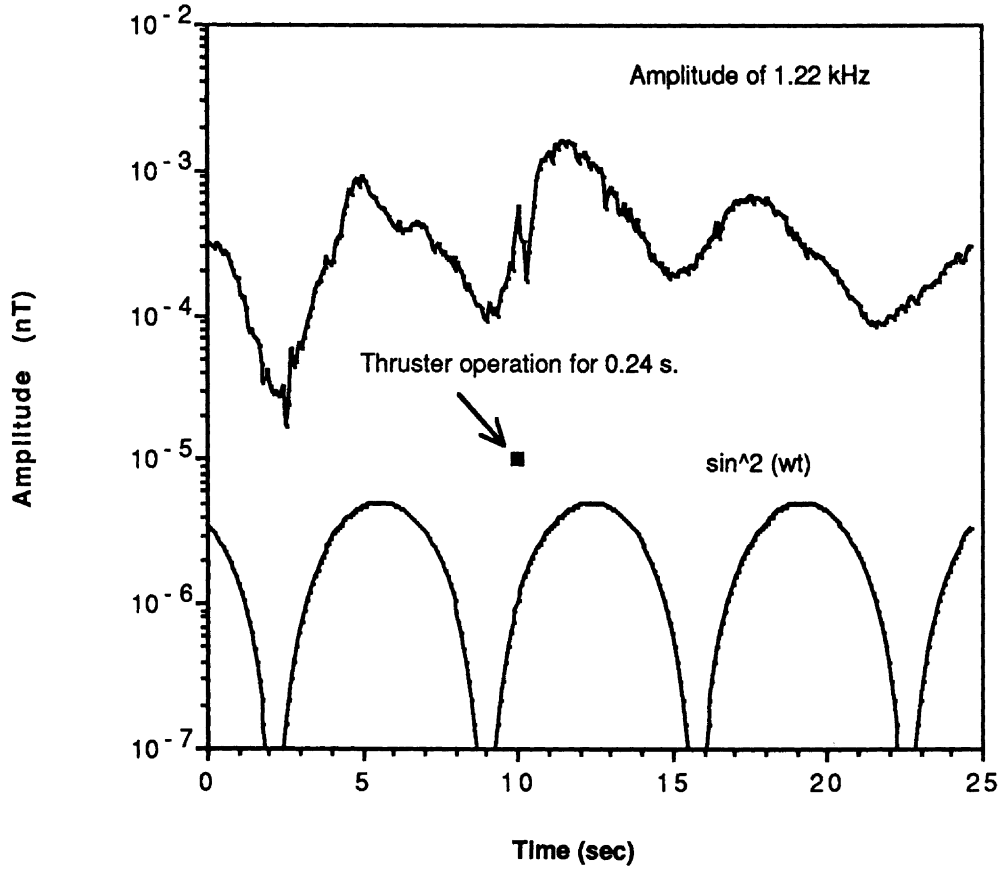


Fig. 4. The amplitude of the 1.22-kHz narrow-band emission observed with the magnetic field search coil plotted as a function of time. Spin modulation of the amplitude due to the rotation of the PDP is observed and may be compared with the function $\sin^2(\omega t)$. A transient disturbance due to the operation of the orbiter thrusters is also observed.

receiver. The broadband emissions dominate the ambient wave fields at all times that the FPEG is firing. In this spectrogram, the strongest emissions are seen between 4 and 8 kHz, near the lower hybrid frequency ($f_{LHR} \approx 6.6$ kHz) and these emissions show spin modulation due to the rotation of the PDP. The effects of thrusters are also observed and are most apparent at 1 and 21 s in the figure. Although it appears that wave activity is diminished, this is only an effect of the AGC. In fact, wave amplitudes are enhanced at all measured frequencies during thruster operations, but the dominance of lower-frequency wave amplitudes suppresses the apparent amplitude at higher frequencies.

*The Pulsed flux tube connection.* The electric field response during the Pulsed flux tube connection is shown in Plate 1*c*. The PDP was at a distance of approximately 210 m parallel and 35 m perpendicular to the conjunction field line, and the FPEG was being modulated at 1.22 kHz. Broadband emissions are observed in all frequency ranges as was the case for dc beam operation. It will be seen below (Figure 5) that the amplitudes of broadband emissions from the pulsed beam are comparable to those from the dc beam but appear less prominent in the spectrograms shown here due to the action of the AGC. Plate 1*c* also shows that the pulsed electron beam produces narrow-band emissions superimposed on the broadband signals. These occur at the beam pulsing frequency of 1.22 kHz and at higher harmonics. The even harmonics are visible but with significantly reduced amplitude, as is predicted by Fourier transform theory for a 50% duty cycle, square-wave-modulated beam.

The PDP was spinning with a period of $\sim$ 13.6 s during its free flight, and many wave emissions show significant amplitude variations as a result. The spin modulation of the broadband and narrow-band emissions is particularly apparent in Plate 1*c*. Since the antennas are symmetric, the PDP spin period gives a wave modulation period of one-half the spin period or 6.8 s. In Figure 4 the magnetic field amplitude of the fundamental (1.22 kHz) is plotted as a function of time along with the function $\sin^2(\omega t)$. From the phase of the modulation and the known position and orientation of the PDP, the polarization of the observed signals can be deduced. The analysis is, however, complicated by secondary instrumental effects. It has been found, for example, that the LEPEDEA instrument aboard the PDP can make anomalous periodic changes to the potential of the PDP and that these shifts can affect the wave results [*Tribble et al.*, 1988]. It appears that the spin modulation and instrumental effects can be separated and the polarization of the signals analyzed. Results will be presented in a later paper. Figure 4 also shows perturbations to the wave signals due to thruster operation on the orbiter. In this case the duration of the thruster operation (0.24 s) is much less than the AGC sample rate (1.6 s), so the amplitudes are unreliable.

*The Prox Ops sequence.* The final spectrogram, Plate 1*d*

shows an antenna period from the Prox Ops sequence. At ~ 20 s in the figure, the FPEG is turned on and modulated at 1.22 kHz. Throughout this time the PDP is mounted in the payload bay and the presence of orbiter interference lines below 500 Hz reduces the apparent amplitude of the other emissions. Prior to FPEG turn-on the spectrum is broadband and low amplitude. When the FPEG begins pulsing, narrow-band emissions up to 30 kHz are observed with odd harmonics dominating. Notably absent is the effect of spin modulation which, of course, does not occur when the PDP is mounted in the payload bay.

*Discussion.* The spectrograms shown in Plates 1*a*–1*d* provide an overview of the wave response to electron beam operation but are lacking in some respects. They do not, for example, provide absolute amplitude information, so the wave intensities from one sequence to another or even from one time within a sequence to another cannot be compared. This must come from the more detailed analysis in the next subsection. Also, the Pulsed flux tube connection and the Prox Ops sequences span seven antenna periods, and the DC flux tube connection spans ten. Plate 1 provides only one antenna period from each of the three sequences and cannot show the time evolution for the duration of the sequences.

To quantify the analysis of radiation from the electron beam, the data were numerically processed to compensate for the effects of the AGC. This was done by using the telemetered values of the gain applied to the signal and the preflight calibration of the receiver system. To determine the accuracy of the AGC compensation procedure, the results were compared with the wave amplitudes from the IMP/Helios instrument, which measured wave field amplitudes with a filter bank which was not connected to the AGC. Agreement within a factor of 2 was found at times when the total wave amplitude changed slowly on the scale of the 1.6-s AGC data sample rate. (See Reeves [1988] for a full explanation of the AGC compensation procedure.) It is important to note that, as a result of the Fourier transforming of digitized data, "amplitude," as used in this paper, means the amplitude of a 12-Hz Fourier spectral component. Although one could transform amplitude (in, say, V/m) into spectral amplitude (in V/m $Hz^{1/2}$), this would be appropriate only for the broadband signals but would not apply to narrow-band signals. Because some spectra contain both broadband and narrow-band signals, all amplitudes in the VLF band are the amplitudes of the 12-Hz Fourier components.

The result of the AGC compensation procedure is that absolute wave amplitudes can be obtained. By averaging over time, the average wave spectra (amplitude as a function of frequency) for the sequences can be compared. This has been done for electric and magnetic wave fields for the three sequences, and our results are presented in the following subsection. The long-term variation from one antenna period to another can also be investigated by considering the amplitude in a selected frequency range as a function of time. Results from this analysis are presented for each of the three sequences in the final observation section.

### *Wave Spectra From the Three Sequences*

Using the technique described above, composite spectra have been created showing the calibrated wave response of the plasma to electron beam injection. Figure 5 shows the time-averaged amplitude versus frequency for the DC and Pulsed flux tube connections and for the Prox Ops sequence. In this paper we have used the convention that, where figures are to be compared with the spectrograms such as in Plate 1, time is plotted on the horizontal axis, and frequency is plotted on the vertical axis.

The spectra are complicated by some instrumental and processing effects which deserve consideration. The magnetic spectrum for the DC flux tube connection (Figure 5*a* lower panel) shows these effects most clearly. The spectra are composites produced by adjoining the spectra from the 0–10, 10–20, and 20–30 kHz frequency ranges of the VLF band. They are not measured simultaneously and, for the flux tube connections, the PDP is moving with respect to the conjunction field line. Therefore there can be discontinuities at 10 and 20 kHz. There is also an effect due to the receiver filter sensitivity. In the 0–10 kHz range the filter function is fairly flat from 0.9 to nearly 10 kHz. From 0.9 down to 0.4 kHz there is some roll-off (as is verified by comparison with the ELF band data), and below 0.4 kHz the signal is dominated by spurious noise. The 10–20 and 20–30 kHz ranges were heterodyned down into the 0–10 kHz range and then rescaled for display. As noted, the 10–20 kHz range was also inverted in frequency. Thus the "lower end" of the filter response is seen near 20 kHz for both frequency ranges and is the explanation for the noise at those frequencies. In addition it is seen that the frequency response of the heterodyned signals is not as flat as it is for the 0–10 kHz frequency range although this effect is considerably reduced for the Prox Ops sequence, which measured more intense signals and was not spinning or moving in time.

There are also narrow-band signals which are attributable to instrumental effects. Virtually all the narrow-band emissions observed in the spectra for the DC flux tube connection are instrumental in origin. The most prominent of these is seen in the magnetic spectrum at 11.5 kHz which is likely to be from a source on the PDP. The slightly broader signal at 24.8 kHz is spin modulated and has an amplitude which varies with distance from the conjunction field line and hence is likely to originate on the orbiter. In addition there are small-amplitude, narrow-band signals which can be found at 1.1 or 2.2 kHz from the "lower end" of the 10-kHz-wide frequency bands. They are clearly instrumental and have not been investigated in detail. We can note that when the PDP is mounted in the payload bay, there is a considerable magnetic, narrow band noise which complicates the appearance of the magnetic spectra. The instrumental effects are also present, but not labeled, in the other spectra in Figure 5.

*The DC flux tube connection.* The relevant orbital and instrumental parameters for this and the other two sequences are given in Table 1. The DC flux tube connection sequence took place at relatively high latitudes during daytime with an ambient electron density of $\sim 10^5$ $cm^{-3}$. Figure 5*a* shows the electric field measured at ~ 50 m from the conjunction field line and the magnetic field measured at ~ 25 m while the electron beam is operated in dc mode with a current of 50-mA. In the VLF range at these locations, broadband electric and magnetic emissions are generated by the beam. The electric field wave amplitudes fall in the range $10^{-8}-10^{-6}$ V/m and the magnetic amplitudes are between $2\times10^{-7}$ and $2\times10^{-5}$ nT. The amplitude of the signals, at

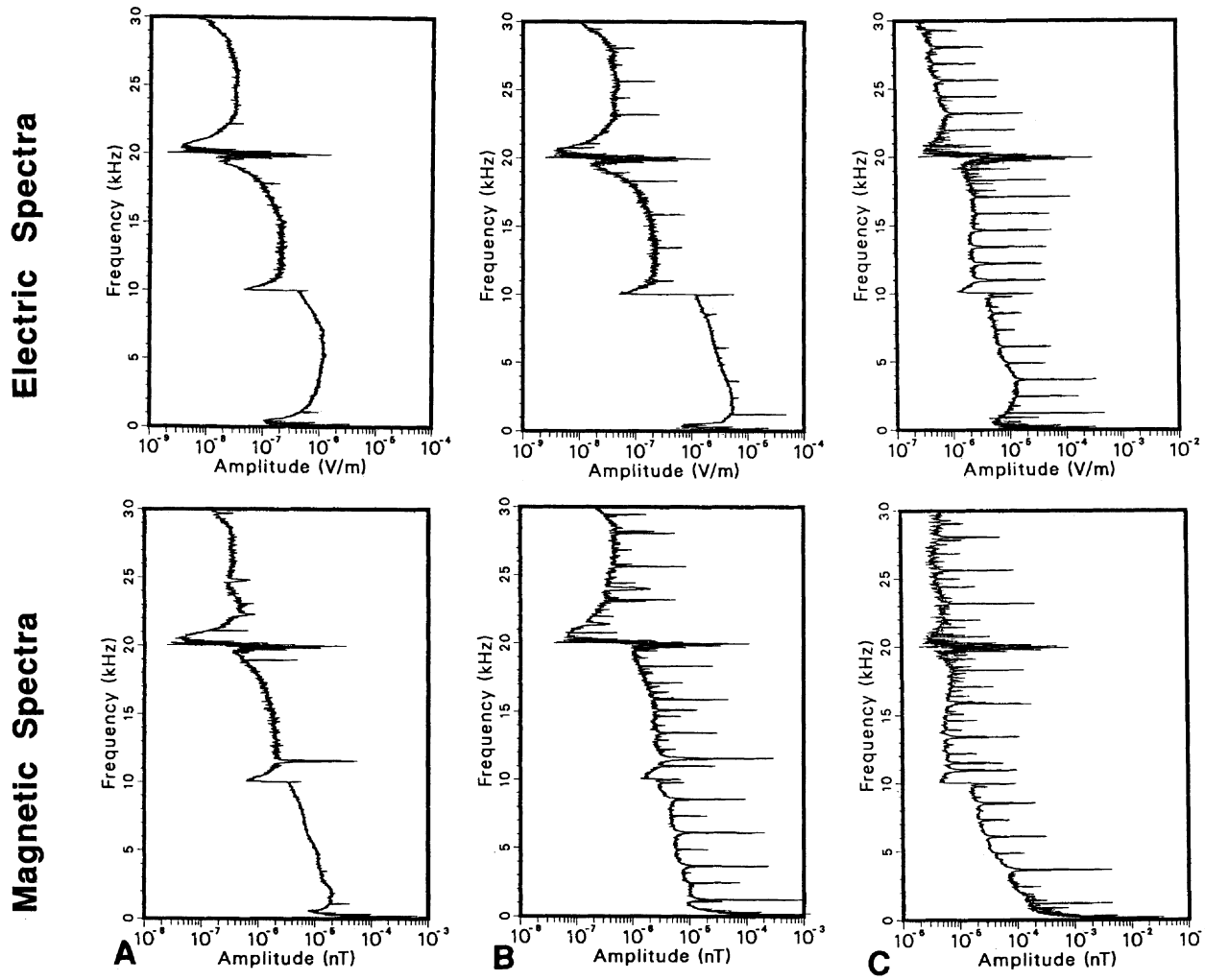


Fig. 5. The 0-30 kHz wave spectra for (*a*) the DC flux tube connection, (*b*) the Pulsed flux tube connection, and (*c*) the Prox Ops sequence. The upper plots in each figure show the electric field amplitude (in volts per meter) versus frequency. The lower plots show magnetic field amplitude (in nanoteslas) versus frequency. To facilitate comparison with the spectrograms of Plate 1, frequency is plotted on the vertical axis.

this distance, decreases with frequency, at a steady rate, up to the 30-kHz limit of the receiver. The ratio of $c\langle B\rangle/\langle E\rangle$ (where angle brackets denote time average) is of order 1 for these antenna periods. The ratio $c\langle B\rangle/\langle E\rangle$ is fairly constant with frequency but is found to vary with distance to the conjunction field line.

*The Pulsed flux tube connection.* The spectra for two antenna periods during the Pulsed flux tube connection are shown in Figure 5*b*. The electric and magnetic field measurements were made at perpendicular distances of approximately 35 and 70 m respectively. It is notable that the broadband signals from the 100-mA, 50% on-time, pulsed electron beam are comparable in amplitude to the 50-mA, 100% on-time, dc electron beam for both the electric and the magnetic fields and at all frequencies measured. The narrow-band emissions are considerably stronger than the broadband emissions. Narrow-band wave amplitudes lie between $5 \times 10^{-8}$ and $5 \times 10^{-4}$ V/m for the electric antenna and between $10^{-6}$ and $10^{-3}$ nT for the magnetic antenna. The amplitudes of the narrow-band emissions generally decrease with frequency but show a greater variation than the broadband emissions. The narrow-band emissions are more electromagnetic with $c\langle B\rangle/\langle E\rangle$ of order 10.

*The Prox Ops sequence.* During the Prox Ops sequence the electron beam was modulated at 1.22 kHz, 100 mA, 50% duty cycle, and the PDP was mounted in the payload bay. The spectra are shown in Figure 5*c*. We see that the broadband emissions again have $c\langle B\rangle/\langle E\rangle$ of order 1 and have a similar spectral shape to the broadband emissions from the DC and Pulsed flux tube connection sequences. However, the emissions are an order of magnitude stronger due to the proximity of the PDP to the FPEG (6.62 m). The narrow-band emissions again show strong response at the pulsing frequency and its harmonics, but $c\langle B\rangle/\langle E\rangle$ is only of order 1. Some of the variation of harmonic structure is seen by comparing the amplitudes of the even harmonics with those measured during the Pulsed flux tube connection. The magnetic field amplitudes are quite similar, but the electric field amplitudes during the Prox Ops sequence are considerably enhanced. This is not simply a result of the

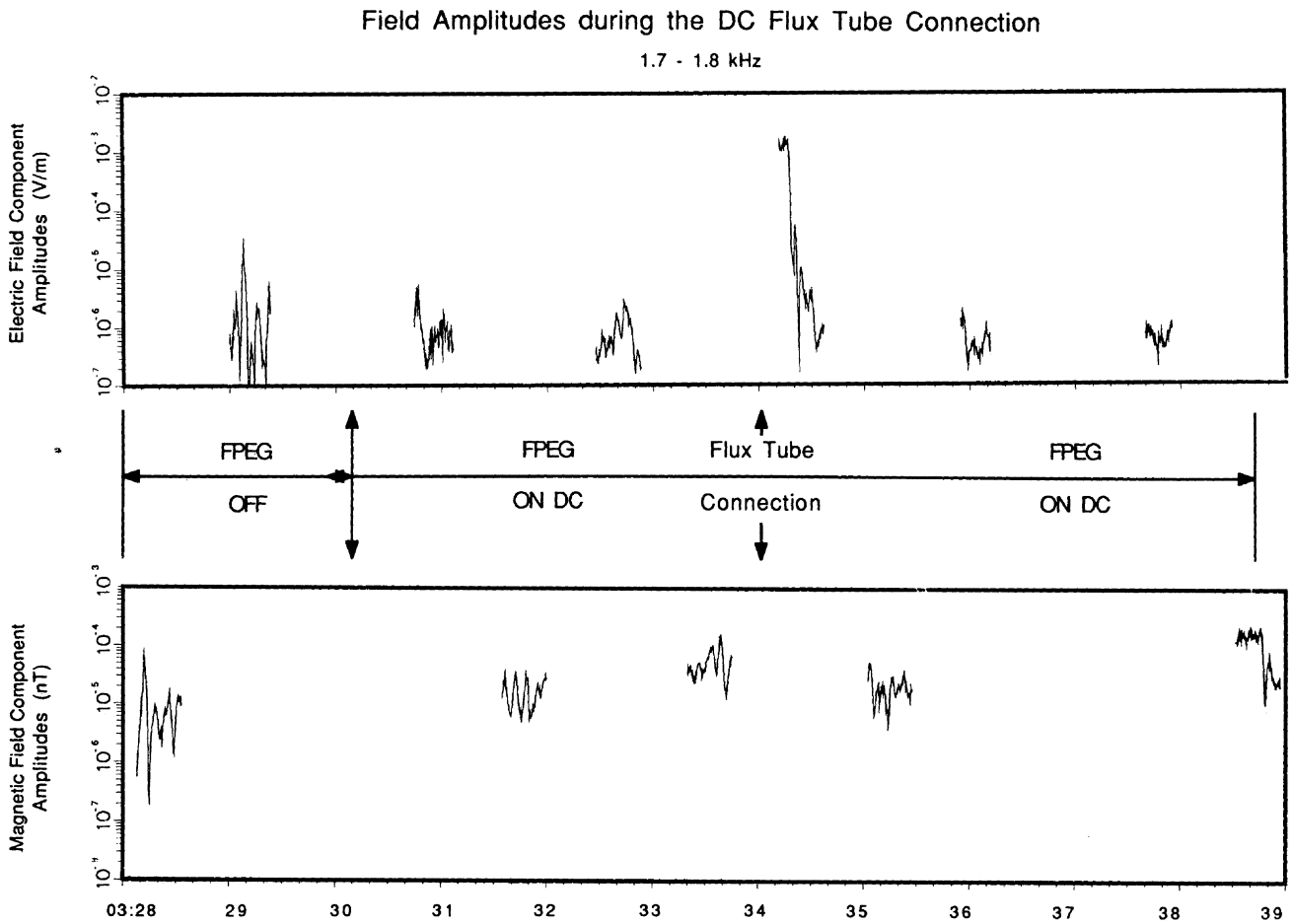


Fig. 6. The amplitude of ( top) electric and (bottom) magnetic field components in the frequency range 1.7–1.9 kHz as a function of universal time for the DC flux tube connection sequence. The trajectory of the PDP is shown in Figure 1. Three zones of beam-generated wave emissions and the region of ambient wave fields may be identified with various amplitudes. Gaps in the wave data are times when the wave receiver is observing waves in the 10–30 kHz frequency range.

PDP being in the payload bay since a variety of harmonic structures are observed with the PDP both mounted and free-flying.

*The Time Variation of Wave Amplitudes*

Investigation of the long-term evolution of the wave amplitudes as a function of time was made. To do this, the data were processed to extract the average amplitude in the frequency band 1.7–1.8-kHz. The frequency range 1.7–1.8 kHz was chosen because it lies between harmonics of 1.22 kHz and contains only broadband emissions but is near enough in frequency to the 1.22 kHz fundamental frequency so a comparison of broadband and narrow-band amplitudes can be made.

Data were extracted for all the antenna periods which measured the 0–10 kHz range during the DC and Pulsed flux tube connections. The average wave amplitude in the frequency range 1.7–1.8 kHz is shown as a function of time for the DC flux tube connection (Figure 6) and for the Pulsed flux tube connection (Figure 7).

*The DC flux tube connection.* The DC flux tube connection data starts at day 213, 0328 UT. At this time the orbiter is on the Earth's dayside. The PDP passes closest to the conjunction field line at approximately 0334:01 UT, and this is referred to as the "flux tube connection." The sequence ends at 0339 still in daytime conditions. During both flux tube connection sequences, the electron beam is freely escaping and has a pitch angle given by the angle between the magnetic field line and a line connecting the orbiter and the PDP. (See Figure 1.) The electron beam emission began at 0330:12. Before this time the PDP measured highly time varying ambient fields. As was the case for the Pulsed flux tube connection, the strongest emissions are due to natural whistlers and to the effects of the orbiter thrusters. (See Plate 1*a*.)

When the FPEG is turned on, the measured fields become more structured with the second magnetic and third electric antenna periods showing the most clear spin modulation of the signals. The electric field amplitudes show less structure, but the average field amplitudes are only slightly enhanced above the pre-gun-turn-on levels of about $10^{-6}$ V/m. The magnetic field amplitudes are also enhanced above background levels but still lie close to the range of $5 \times 10^{-6}$ nT seen before FPEG turn-on to $5 \times 10^{-5}$ nT after FPEG turn-off. While the FPEG is on, field amplitudes remain fairly

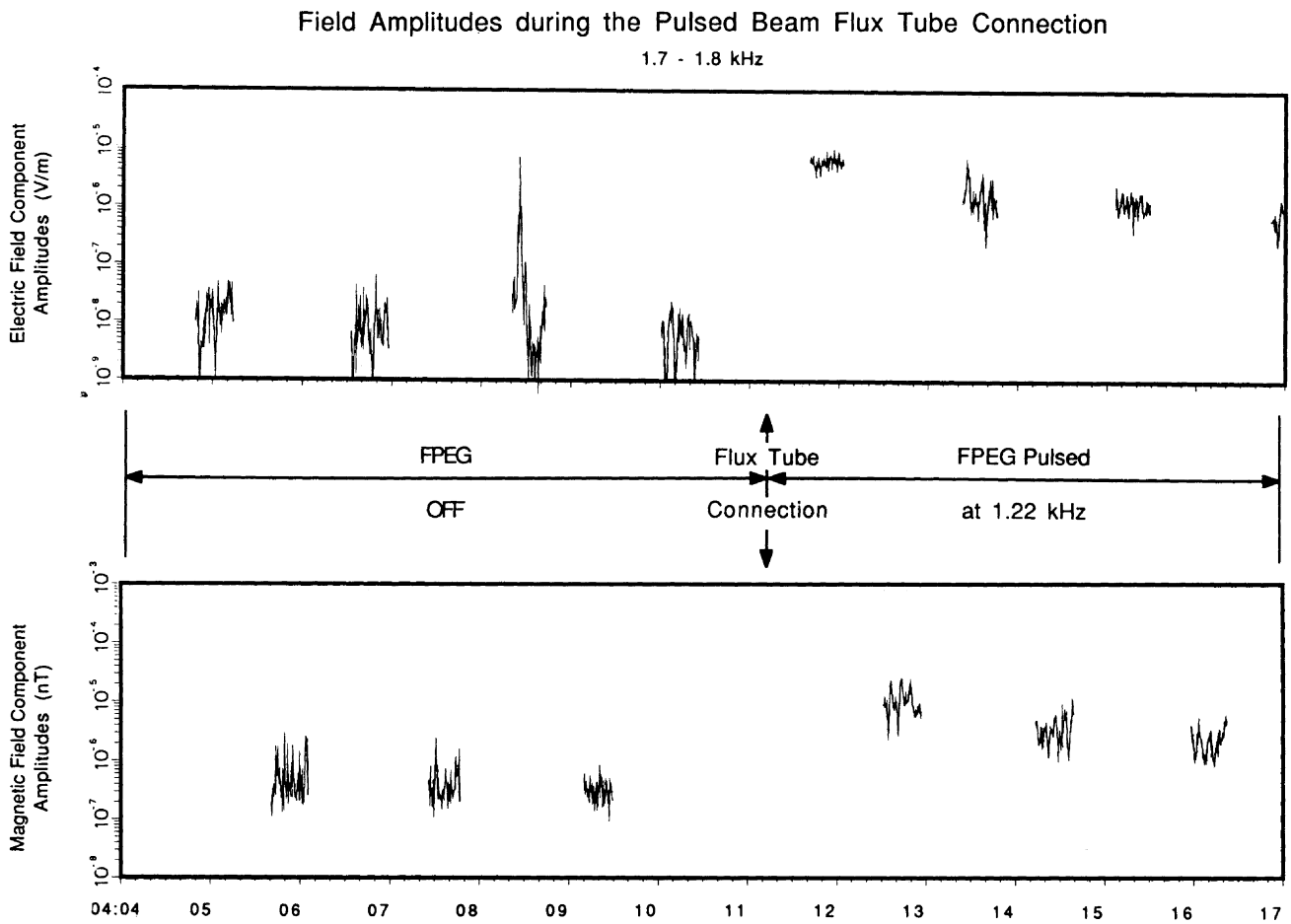


Fig. 7. The amplitude of ( top) electric and (bottom) magnetic field components in the frequency range 1. 7–1.9 kHz as a function of universal time for the Pulsed flux tube connection sequence. The trajectory of the PDP is shown in Figure 1. At the time of closest approach to the conjunction field line the FPEG is turned on. The wave receiver was connected to the Langmuir probe at this time, and there is an additional gap in the wave data.

constant with the exception of the fourth electric antenna period, when intense electric fields are measured which saturate the automatic gain control for nearly 10 s and then drop rapidly back down to the $10^{-6}$ V/m level. The strongest signal was measured when the PDP was at its closest approach to the conjunction field line. This distance has been calculated to be less than 5 m.

*The Pulsed flux tube connection.* The Pulsed flux tube connection data start on day 213 at 0404 UT, last for 13 min, and take place on the nightside of the Earth. For this sequence, the FPEG is off throughout the period of approach to the conjunction field line and is turned on when the PDP is near its closest approach, unfortunately while the wideband receiver is connected to the Langmuir probe, preventing the acquisition of wave data. The FPEG is then on for the remainder of the sequence while the PDP completes a trajectory very similar to that for the DC flux tube connection (Figure 1). We see that the ambient fields, measured with the FPEG off, are nearly 100 times weaker for the electric and 10 times weaker for the magnetic field measurements. As seen from the spectrograms in Plate 1, the ambient fields, although slightly spin modulated, are dominated by natural whistlers and thruster wave effects as they were in the dc case. With the FPEG on we see enhanced electric and magnetic field amplitudes that drop off as the PDP moves away from the conjunction field line. The electric field amplitudes at about 100 m perpendicular distance from the beam are of the order of $10^{-6}$ V/m and the magnetic field amplitudes range from $10^{-6}$ to $10^{-5}$ nT. These values are very nearly the same as the amplitudes of broadband emissions in the dc case and, as we have seen, the amplitude of broadband emissions during the two flux tube connections tend to be the same for all frequencies in the 0–30 kHz range.

For the Pulsed flux tube connection we can also compare the dependence of field amplitude as a function of distance from the conjunction field line for narrow-band as well as broadband emissions. This dependence is shown in Figure 8*a* for the electric antenna and Figure 8*b* for the magnetic antenna. The amplitude plotted is the amplitude averaged over the 26-s duration of the 0–10 kHz frequency range, and the distance is the average distance during that period. The electric field amplitude of the narrow-band emission at 1.22 kHz is 5 times stronger than the average broadband amplitude in the 1.7–1.9 kHz frequency range, and the magnetic field amplitude at 1.22 kHz is 15 times stronger than the broadband amplitudes. This ratio stays fairly constant and thus relatively independent of where the wave field is measured.

It should be noted that a comparison of broadband and

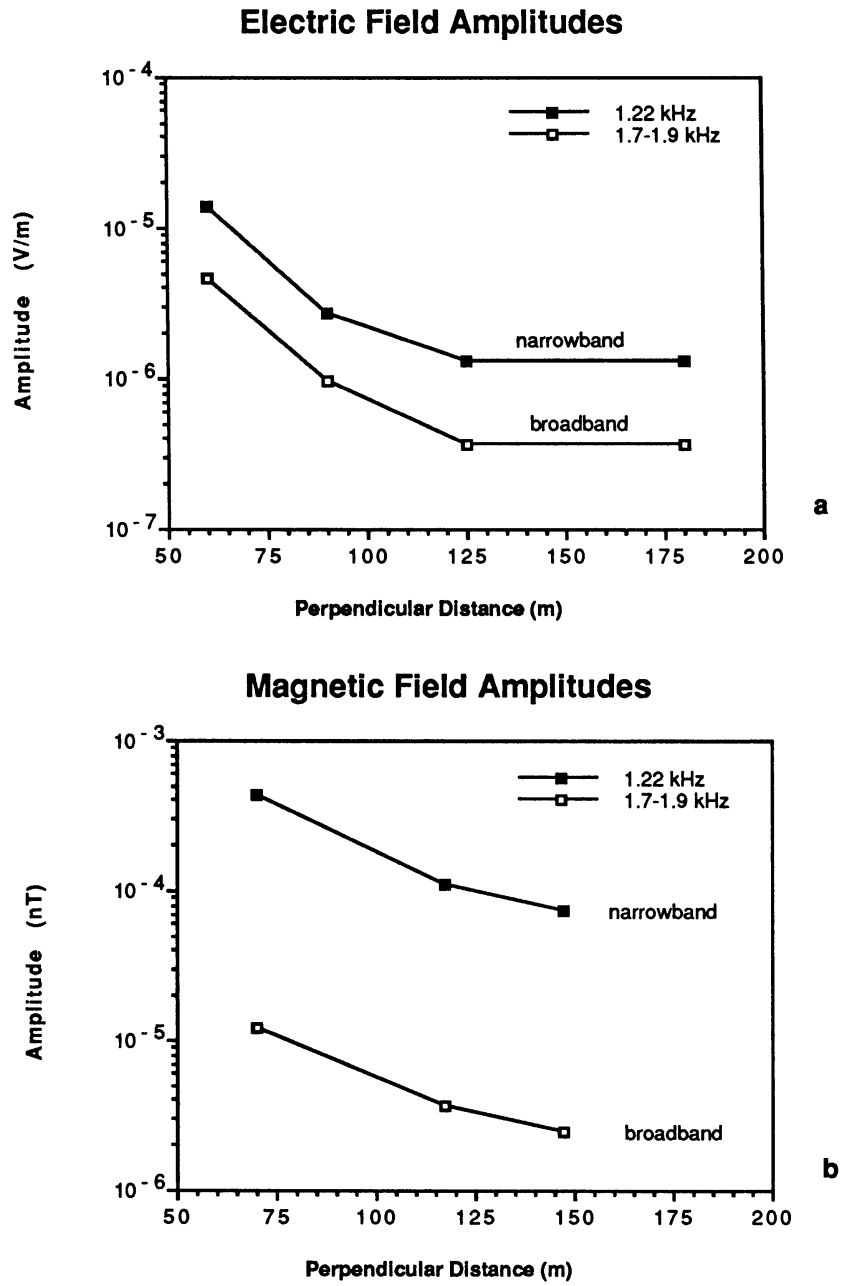


Fig. 8. A comparison of narrow-band and broadband field strengths as a function of perpendicular distance to the conjunction field line during the Pulsed flux tube connection as measured by the (*a*) electric dipole antenna and (*b*) the magnetic search coil antenna. The ratio of amplitudes is observed to be a fairly constant function of distance from the conjunction field line.

narrow-band emissions at higher harmonic frequencies shows different behavior because the harmonic structure of the narrow-band emissions varies in time and/or distance. Figure 9 shows the harmonic structure at four distances for the electric antenna (Figure 9*a*) and at three distances for the magnetic antenna (Figure 9*b*). One interesting feature is that for greater distances from the conjunction field line, the electric field amplitudes of the second and third harmonics are larger than the amplitude of the fundamental. The magnetic field data do not display this behavior but instead show the even harmonics (the "forbidden" frequencies) at greatly reduced amplitudes for all distances. The unexpected strength of the second and third harmonic electric field amplitudes at large distances may be due to their proximity to the lower hybrid resonance frequency, which is approximately 3.6 kHz for the conditions during the Pulsed flux tube connection.

*The Prox Ops sequence.* The Prox Ops sequence begins on day 212 in sunlight. The orbiter velocity vector was directed toward the nose and slightly down (below the plane of the wings) so the payload bay was in light wake conditions. (See Table 1.) At 1831:42 UT the electron beam was turned on, and the electric field broadband and narrow-band amplitudes increased over previous background levels by roughly a factor of 10 and 100 respectively (Figure 10). The amplitude of broadband and narrow-band emissions stays fairly

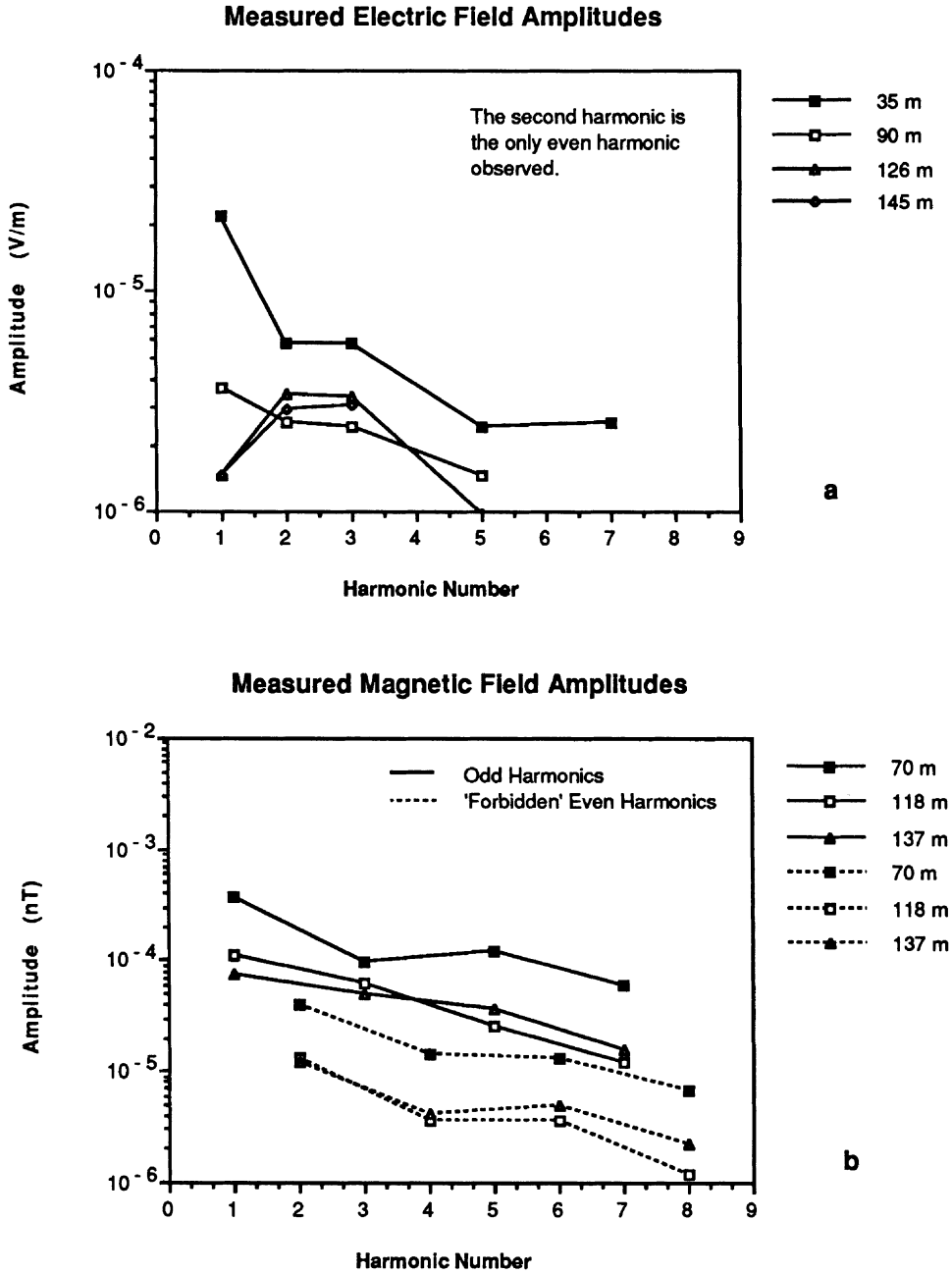


Fig. 9. The measured (*a*) electric and (*b*) magnetic field harmonic structure during the Pulsed flux tube connection at various distances from the conjunction field line. For distances greater than 100 m the electric field amplitudes of the second and third harmonics are observed to be slightly enhanced. For the magnetic field measurements the even, forbidden harmonics are plotted with dashed lines and are observed to be of significantly lower amplitude than the odd harmonics.

constant up to 1835:15 UT when the electron beam was determined to have hit the orbiter starboard payload bay door. We observe that the amplitudes of both the narrow-band and the broadband electric emissions abruptly increase at this time while the magnetic field amplitudes do not. When the FPEG turns off at 1836:52 UT, the broadband signals are at their presequence levels while the 1.22-kHz signals are an order of magnitude higher indicating that the orbiter environment is still "ringing" at the pulsing frequency. The spectra shown in Figure 5c are from the earlier portion of the sequence when the electron beam was escaping. Spectra from the later portion of the sequence are considerably different with the 0–10 kHz, even and odd harmonics of comparable amplitude (Figure 11).

## 4. Discussion

### *Comparison With STS 3/OSS 1*

The wave spectra from pulsed electron beam operations on Spacelab 2 were found to confirm and extend the results from the STS 3/OSS 1 mission [*Reeves et al.*, 1988].

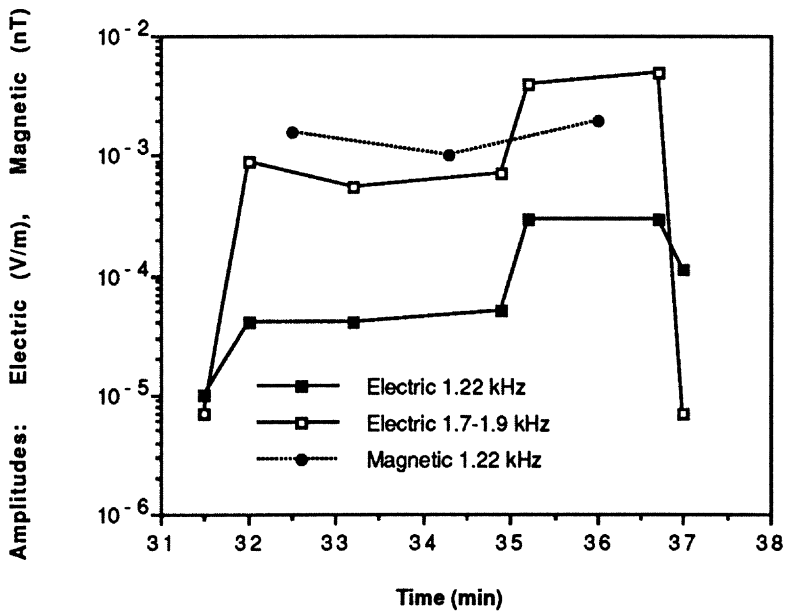


Fig. 10. The time variation of the electric and magnetic field amplitudes during the Prox Ops sequence showing the increase in electric field strength when the beam is turned on and the further increase when the electron beam hits the orbiter instead of propagating away from the orbiter. The amplitude of the 1.22-kHz emission observed with the magnetic antenna does not increase when the beam hits the orbiter.

Broadband electromagnetic emissions are produced by beam operations, and narrow-band emissions at the pulsing frequency and its harmonics are observed both during the free flight and when the PDP was mounted in the payload bay (as it was for STS 3). The harmonic structure of narrow-band emissions varies from one sequence to another. As in Plate 1*c*, it is often observed that narrow-band frequencies for which $\sin(\gamma\pi\, b/d) = 0$ (where $\gamma$ is the harmonic number and $b/d$ is the duty cycle) are not observed or are observed with significantly reduced amplitudes. For this reason, these frequencies are referred to as "forbidden frequencies." The presence of emissions at the forbidden frequencies is thought to reflect a loss of coherence of the square-wave structure of the current source, as will be discussed further below.

An important observation from STS 3/OSS 1 was the detection of "satellite lines" and "subharmonics." Satellite lines were identified as narrow-band emissions associated with the harmonics of the beam pulsing frequency. Dur-

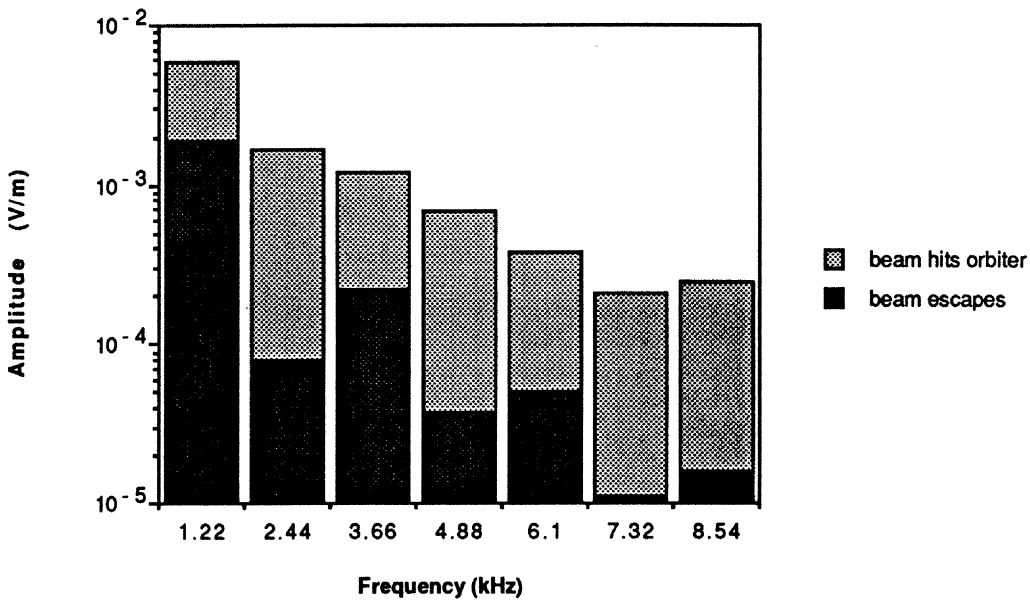


Fig. 11. A comparison of the amplitudes of narrow-band harmonics of the 1.22-kHz pulsing frequency during the Prox Ops sequence. When the beam is freely escaping from the orbiter, the even "forbidden" harmonics appear with significantly reduced amplitude compared to the odd harmonics. When the beam hits the orbiter, its square-wave current structure is lost, and the even harmonics appear with amplitudes which are comparable to the amplitudes of the odd harmonics.

ing the STS 3 mission, they were often observed in conjunction with harmonics particularly in the higher frequency ranges (20–30 kHz). The difference between the frequency of the harmonic and the satellite line ($\Delta f$) was found to be the same for each harmonic which had an associated satellite line, but $\Delta f$ itself varied with time. Subharmonics are narrow-band emissions observed well below the pulsing frequency, usually in the ELF band. It was found that the frequency of the subharmonics ($f_{sub}$) was equal to the difference in frequencies between the satellite lines and the harmonics ($f_{sub} = \Delta f$). (See Figure 9 of *Reeves et al.* [1988].) Satellite lines and subharmonics have been observed on the Spacelab 2 mission during the Pulsed flux tube connection sequence. As with STS 3, it was observed that the satellite lines are more commonly associated with higher harmonics, that $f_{sub} = \Delta f$, and that $f_{sub}$ and $\Delta f$ vary in time. These observations are mentioned here for completeness. An analysis of the production of satellite lines and subharmonics will appear in a later publication.

The results from the STS 3/OSS 1 mission presented by *Reeves et al.* [1988] and preliminary observations from Spacelab 2 presented by *Bush et al.* [1987] were primarily qualitative observations of the characteristics of electron beam wave generation. The development of a technique for extracting wave amplitude from the broadband data has allowed for a more quantitative discussion for the results of Spacelab 2.

*Broadband Emissions From Pulsed and DC Electron Beams*

Figures 5, 6, and 7 reveal some basic information about the amplitude of broadband emissions generated by electron beams in space plasmas. It appears that dc and pulsed electron beams that deliver the same power into the plasma medium produce broadband emissions of comparable amplitude and comparable spectral shape when measured at similar locations with respect to the magnetic field line along which the electron beam propagates. The background fields during the DC flux tube connection were considerably stronger than the background fields during the Pulsed flux tube connection. When the FPEG is on, the measured field amplitudes range from saturated values at locations very near the conjunction field line to $10^{-6}$ V/m and $10^{-6}$–$10^{-5}$ nT at larger distances from the conjunction field line. In the case of the DC flux tube connection, the amplitudes of beam-generated electromagnetic fields at larger distances are of the same order as the background fields, while for the Pulsed flux tube connection, the beam-generated fields are above the background levels at all points of measurement. Although, as we would expect, the amplitude is a function of the frequency and the position at which the wave field is measured, we can make some general comments about broadband wave production by electron beams propagating along magnetic field lines in the ionosphere.

From Figures 6 and 7 we identify three zones of wave amplitude. Zone 1 occurs very near the conjunction field line and is a narrow region of very intense wave activity. Zone 2 spans a somewhat wider region of space than zone 1 and is characterized by a very rapid decrease in amplitude with increasing distance from the conjunction field line. Zone 3 contains wave fields that are of significantly lower amplitude than those in zones 1 and 2 but often above the amplitude of ambient, background wave activity.

Zone 1 is a region of very disturbed plasma which exists in a region near the electron beam and in the wake of the beam. For the DC flux tube connection, zone 1 extends approximately 20 m in diameter, which is somewhat larger than the region in which the beam is expected to be propagating. It is characterized by a very turbulent plasma environment which makes measurement of temperature and density unreliable. As observed, it is also a region of intense wave activity which saturated the wideband receiver. These waves include the Cherenkov, resonance cone radiation which at higher frequencies produces the funnel-shaped emissions observed by *Gurnett et al.* [1986]. At frequencies below 30 kHz those waves propagate at less than 5° to the magnetic field and thus occupy a region of very small spatial extent. In Figure 6, the zone 1 emissions are observed at ~ 0334:10–0334:20 UT.

The waves in zone 2 can also be identified in Figure 6. Zone 2 surrounds zone 1, and therefore, zone 2 emissions are observed in Figure 6 from 0334:20 UT until the antenna switches off the 0–10 kHz range at ~ 0334:40 UT. In that interval the amplitude of broadband waves in the range 1.7–1.8 kHz drops from ~ $10^{-4}$ to ~ $10^{-6}$. From observations of the broadband amplitude in different frequency ranges it is found that the spatial extent of zone 2 varies with frequency. In general, waves with frequencies below 1 kHz have a larger spatial extent than waves with frequencies above 1 kHz. Although the antenna switching pattern did not allow for measurement in the range 1.7–1.8 kHz, the ELF band measured the broadband magnetic fields just prior to the flux tube connection point. Observations in this range show that the magnetic field amplitudes are also enhanced in the zone 2 region, indicating that there is an electromagnetic component to those waves. Although comparison of broadband electric and magnetic field components in most of the region of observation gives $c\langle B\rangle/\langle E\rangle$ of order 1, comparison of zone 2 emissions in the ELF range gives a ratio of order 10. Analysis indicates that the electromagnetic components may be waves generated through the Cherenkov resonance with wave normal angles in the central hump of the index of refraction surface (G. D. Reeves et al., VLF wave emissions by pulsed and dc electron beams in space, 2. Analysis of Spacelab 2 results, submitted to *J. Geophys. Res*, 1988; hereafter G. D. Reeves et al., submitted manuscript, 1988).

Zone 3 includes the other two zones but is considerably larger in spatial extent. Although the transition from zone 2 to zone 3 is smooth rather than abrupt, zone 3 emissions can be distinguished as a distinct part of the wave field. It is characterized by the observation of broadband emissions which are not highly time varying and which drop off in amplitude with increasing distance from the conjunction field line but at a much slower rate than the emissions in zone 2. During the DC flux tube connection sequence, the amplitudes of zone 3 emissions are only slightly higher than the ambient levels of ~ $10^{-6}$ V/m and $10^{-5}$ nT. During the Pulsed flux tube connection sequence, however, the ambient wave amplitudes were ~ $10^{-8}$ V/m and $10^{-6}$ nT. Therefore the zone 3 emissions are most apparent in Figure 7 where they are observed to have both electric and magnetic components which decrease in amplitude with distance.

*Narrow-Band Emissions*

We have seen that the amplitudes of narrow-band emissions produced by pulsed electron beams share some of the same characteristics as broadband emissions. The theory

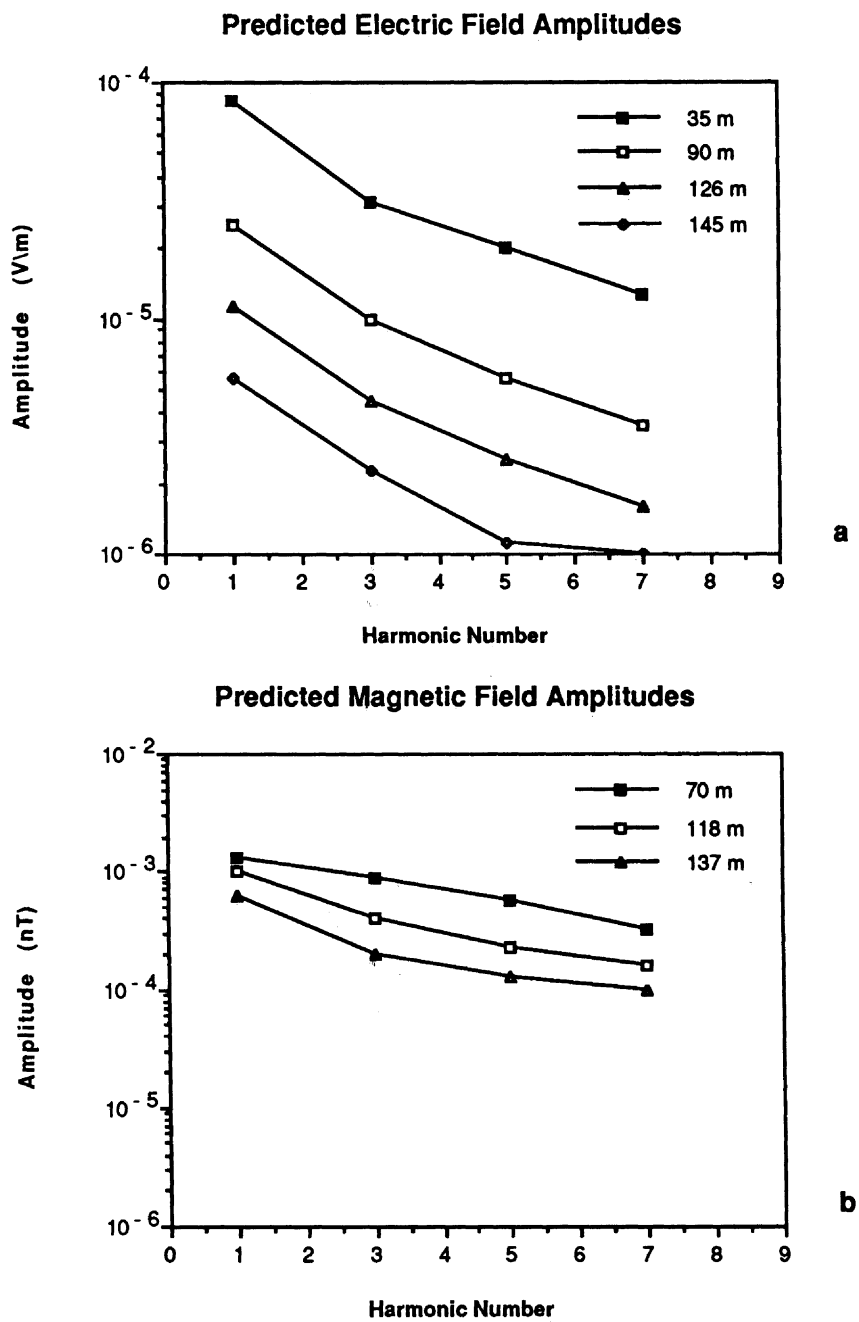


Fig. 12. The (*a*) electric and (*b*) magnetic field amplitudes predicted using the theory of *Harker and Banks* [1987]. Plots show the predicted amplitude for the $s = 0$, Cherenkov resonance with $\theta < \theta_{res}$ as a function of harmonic number. The measured magnetic field strength, electron density, and pitch angle appropriate for the Pulsed flux tube connection were used for the calculation. Comparison with the measured amplitudes (Figure 9) shows fairly good agreement.

of *Harker and Banks* [1987] was developed to predict the electric field amplitudes of narrow-band, near-field radiation from pulsed electron beams in space. *Neubert and Harker* [1988] extended this theory to narrow-band magnetic field amplitudes. A detailed comparison of the observed and predicted amplitudes of the narrow-band radiation can be found in the paper by G. D. Reeves et al. (submitted manuscript, 1988). There it is shown that the best agreement between observation and theory occurs for the predictions for Cherenkov radiation with wave normal angles less than the resonance cone angle. The predicted wave amplitudes for the conditions during the Pulsed flux tube connection sequence are presented in Figure 12. The electric and magnetic field amplitudes are plotted versus harmonic number for the distances at which measurements were made. Comparison of Figures 12 and 9 shows that the observed wave amplitudes for the odd harmonics are somewhat lower than those predicted by theory but are comparable in amplitude and spectral shape. The theory does not predict amplitudes for the even harmonics because of the assumption of perfect square-wave coherence.

*The harmonic structure of narrow-band emissions.* The prediction that the even harmonics are "forbidden" is specific to the case of an electron beam which is pulsed with

a 50% duty cycle. In general, any harmonic for which the harmonic number times the duty cycle of the beam pulse is integral will be predicted to be forbidden. This is a result of the Fourier decomposition of the square-wave shape of the electron beam current and is independent of the details of the calculation. We observe that the even harmonics have a substantially reduced magnetic component but that the electric component may have an amplitude which exceeds the amplitude of the odd harmonics (Figures 5 and 9). The presence of narrow-band harmonics at the forbidden frequencies is most likely due to a degradation in the coherence of the beam making the assumption of a perfect square-wave current source invalid. This possibility is supported by an analysis of the harmonic structure during the Prox Ops sequence.

During the Prox Ops sequence the PDP measures fields in the orbiter payload bay 6.62 m from the FPEG aperture. Both the broadband and narrow-band amplitudes are therefore higher than those measured during the free flight at times other than the period of AGC saturation in zone 1. During the Prox Ops sequence the PDP is fixed in position. However, the relative orientation of the orbiter with respect to the ambient magnetic field vector changes so that the Prox Ops sequence begins with the electron beam freely escaping the orbiter bay but ends with the beam hitting the orbiter. Using the measured values of the ambient magnetic field strength and direction and the nominal electron beam energy of 1-keV, the trajectory of the electrons can be calculated. This information was used with a three-dimensional computer model of the orbiter and the instruments in the payload bay to determine that, as the magnetic field direction changed from $120^o$ to $114^o$ from the orbiter $z$ axis, the electron beam hit the orbiter on the starboard payload bay door approximately 4 m from the FPEG aperture. The calculations were done assuming each electron in the beam acts independently and follows the classical helical trajectory around the magnetic field. Observations of the electron beam hitting the tail of the orbiter using the low light level TV camera on the OSS 1 mission have shown that this is not the case. Rather, the electrons spread both along and across the magnetic field direction to form a hollow cylinder defined by the gyroradius of the electrons and the magnetic field which will be referred to as the "beam column" [*Banks and Raitt*, 1988]. This spreading takes place within a distance of several meters, so the intersection of the beam column and the orbiter surface is more likely an arc defined by the intersection of the beam column and the payload bay doors. The result of the change in the propagation of the electron beam away from the orbiter is a change in the characteristics of radiation from the electron beam. The fact that electric field amplitudes increase when the electron beam hits the orbiter while the magnetic field amplitudes do not (Figure 10) suggests that the fields measured very close to the beam are near-field, incoherent emissions but that the current distribution still defines the spectral structure. The spectral structure of the narrow-band emissions give some clues as to the radiating portion of the electron beam pulse. When the beam is freely escaping, the spatial distance between two 1.22-kHz pulses is 15 km in free space. When the beam hits the orbiter, its length is only several meters, and the harmonic structure of the beam changes as is shown in Figure 11. It appears that the even harmonics in the 0–10 kHz frequency range become comparable in amplitude to the odd harmonics because the square-wave current structure is lost.

## 5. CONCLUSIONS

The VLF wave observations from the wideband wave receiver on Spacelab 2 confirm and extend the results of electron beam wave stimulation experiments on the STS 3/OSS 1 mission [*Reeves et al.*, 1988]. It was found on both missions that a 1-keV electron beam injected from the space shuttle orbiter produced copious broadband electromagnetic emissions. When the electron beam was square-wave modulated, narrow-band emissions at the pulsing frequency and harmonics of that frequency are observed to be produced along with the broadband emissions. The harmonic structure of the narrow-band emissions was often consistent with the assumption of a square-wave current source but, at times, forbidden frequencies were observed, indicating some loss of coherence in the square-wave structure. Satellite lines and subharmonics with $f_{sub} = \Delta f$ were observed during the Pulsed flux tube connection, but the production of satellite lines does not appear to have been as common during the Spacelab 2 beam firings as during beam firings on the STS 3/OSS 1 mission.

The Spacelab 2 mission included a 6-hour free flight of the PDP which allowed sampling of the wave environment out to several hundred meters from the orbiter. In addition, a technique was developed wherein the broadband analog signal was digitized and the effects of the automatic gain control could be removed. This allowed the determination of absolute wave amplitudes. These two improvements allow more quantitative observations and more detailed analysis of the electron beam wave generation results than was possible for the STS 3 experiments.

It was found that the wave environment at distances of several hundred meters from the orbiter when the FPEG was not firing was dominated by broadband natural atmospherics and orbiter thruster-generated wave disturbances. Ambient wave fields can have amplitudes up to $10^{-6}$ V/m and $10^{-5}$ nT, but the higher-amplitude wave fields tend to be observed mainly in regions of higher ambient plasma density. The broadband ambient wave amplitudes may be spin modulated but are often more highly time varying. Narrow-band, electrostatic, variable frequency emissions are also observed in the ambient wave environment.

During both dc and pulsed electron beam operations, broadband electromagnetic radiation is produced throughout the 0–30 kHz range of the wideband receiver. During the flux tube connections it is possible to observe the wave fields at various locations with respect to the conjunction field line. Three zones of wave activity were identified. Zone 1 occurs closest to the conjunction field line. It is characterized by a region of very turbulent plasma and by large-amplitude waves. These waves saturate the wideband VLF wave receiver and are responsible for the funnel-shaped emission identified by *Gurnett et al.* [1986]. In zone 2, broadband VLF emissions in the range $100 < f < 30,000$ Hz decrease in amplitude very rapidly with increasing distance from the conjunction field line. Zone 3 contains contributions to the wave environment which exist within a few perpendicular wavelengths from the conjunction field line. The amplitude of these emissions, in some cases, still exceeds the amplitude

of waves in the ambient environment, but the amplitudes are less than the amplitudes in zones 1 or 2 and decrease more slowly with distance.

The amplitude of broadband emissions during the Pulsed flux tube connection sequence was found to be approximately equal to those for the DC flux tube connection sequence when measured at similar positions with respect to the conjunction field line. This was true throughout the measured frequency range. These results indicate that 100-mA, 50% duty cycle, pulsed beams produce broadband emissions through the same mechanism as for 100-mA, dc beams.

In addition to broadband radiation, pulsed electron beams produce narrow-band radiation at the pulsing frequency and its harmonics. Comparison of measured amplitudes with predictions using the theory of *Harker and Banks* [1987] for near-field, narrow-band radiation from pulsed electron beams shows good agreement for the $s = 0$, Cherenkov resonance solutions with wave normal angles less than the resonance cone angle ($\theta < \theta_{res}$). The observed waves generally have amplitudes less than those predicted by Harker and Banks but are less than a factor of 30 lower in amplitude than predicted. The observed harmonic structure is consistent with the predictions with the exception of the electric field measurements at distances greater than 100 m from the conjunction field line. For those measurements, the second and third harmonics, which have frequencies near the lower hybrid frequency, appear with slightly enhanced amplitudes. It is interesting to note that the broadband and narrow-band amplitudes near the beam pulsing frequency have the same variation in amplitude with perpendicular distance to the conjunction field line.

The presence of emissions at the forbidden frequencies is not predicted by theory but appears to be the result of loss, or partial loss, of the coherence of the square-wave structure of the current source. In the case of a 50% duty cycle beam pulsing, the even harmonics are forbidden. Observations during the Prox Ops sequence show that when the beam is freely escaping, the amplitude of the forbidden, even harmonics is as much as 2 orders of magnitude lower than the odd harmonics. As the inclination of the Earth's magnetic field with respect to the orbiter changed during the Prox Ops sequence, the electron beam hit the orbiter payload bay doors instead of escaping. At this time the wave amplitudes measured in the payload bay increased and the harmonic structure changed such that forbidden, even harmonics appeared with amplitudes equal to the amplitude of the odd harmonics. It is believed that this is the result of the inability of the beam to maintain square-wave structure. In general it is found that observations of the magnetic field components at the forbidden frequencies are in better agreement with theory and that the harmonics at forbidden frequencies are more electrostatic than the other harmonics.

*Acknowledgments.* The authors would like to thank L. Frank and K. J. Harker for their valuable contributions. This work was conducted at Stanford University under NASA grant NAGW-225.

The Editor thanks R. W. Fredricks and another referee for their assistance in evaluating this paper.

## REFERENCES

Akai, K., Electron beam-plasma interaction experiment in space, *Res. Note 285*, Inst. of Space and Astronaut. Sci., Tokyo, 1984.

Banks, P. M., and W. J. Raitt, Observations of electron beam structure in space experiments, *J. Geophys. Res., 93*, 5811, 1988.

Banks, P. M., W. J. Raitt, A. B. White, R. I. Bush, and P. R. Williamson, Preliminary results from the Vehicle Charging and Potential experiment on STS 3, *J. Spacecr. Rockets, 24*, 138, 1987.

Banks, P. M., W. J. Raitt, P. R. Williamson, T. Neubert, R. I. Bush, J. G. Hawkins, G. R. Reeves, and B. White, Results of vehicle charging, plasma densities, and wave generation experiments on Spacelab 2, Banks, P. M., and W. J. Raitt, Observations of electron beam structure in space experiments, *J. Geophys. Res., 93*, 5811, 1988.

Banks, P. M., W. J. Raitt, P. R. Williamson, T. Neubert, R. I. Bush, J. G. Hawkins, G. R. Reeves, and B. White, Results of vehicle charging, plasma densities, and wave generation experiments on Spacelab 2, *J. Spacecr. Rockets*, in press, 1988.

Beghin, C., J. P. Lebreton, B. N. Maehlum, J. Troim, P. Ingsoy, and J. L. Michau, Phenomena induced by charged particle beams., Science, 225, 1984.

Bilitza, D., International reference ionosphere: Recent developments., *Radio Sci., 21*, 343, 1986.

Bush, R. I., G. D. Reeves, P. M. Banks, T. Neubert, P. R. Williamson, W. J. Raitt, and D. A. Gurnett, Electromagnetic fields from pulsed electron beam experiments in space: Spacelab 2 results, *Geophys. Res. Lett., 14*, 1015, 1987.

Cai, D., T. Neubert, L. R. O. Storey, P. M. Banks, S. Sasaki, K. Abe, and J. L. Burch, ELF oscillations associated with electron beam injections from the space shuttle, *J. Geophys. Res., 92*, 12, 451, 1987.

Farrell, W. M., D. A. Gurnett, P. M. Banks, R. I. Bush, and W. J. Raitt, An analysis of the whistler mode radiation from the Spacelab 2 electron beam, *J. Geophys. Res., 93*, 153, 1988.

Gendrin, R., The French-Soviet ARAKS experiment, *Space Sci. Rev., 15*, 905, 1974.

Gurnett, D. A., W. S. Kurth, J. T. Steinberg, P. M. Banks, R. I. Bush, and W. J. Raitt, Whistler mode radiation from the Spacelab 2 electron beam, *Geophys. Res. Lett., 13*, 225, 1986.

Harker, K. J., and P. M. Banks, Near fields in the vicinity of pulsed electron beams in space, *Planet. Space Sci., 35* 11, 1987.

Hawkins, J. G., Vehicle charging and return current measurements during electron beam emission experiments from the shuttle orbiter, Ph. D. dissertation, Stanford Univ., Stanford, Calif., 1988.

Hayakawa, M., Y. Tanaka, K. Ohta, and J. Okuda, Absolute intensity of daytime whistlers at low and middle latitudes and its latitudinal variation, *J. Geophys., 59*, 67, 1986.

Helliwell, R. A., *Whistlers and Related Atmospheric Phenomena*, Stanford University Press, Stanford, Calif., 1965.

Hess, W. N., Generation of artificial aurora, *Science, 164*, 1512, 1969.

Holzworth, R. H., and H. C. Koons, VLF emissions from a modulated electron beam in the auroral ionosphere, *J. Geophys. Res., 86*, 853, 1981.

Jacobsen, T. A., and N. C. Maynard, Polar 5–An electron accelerator experiment within an aurora 3. Evidence for significant spacecraft charging by an electron accelerator at ionospheric altitudes, *Planet. Space Sci., 28*, 291, 1980.

Meltzner, F., G. Metzner, and D. Antrack, The GEOS electron beam experiment S 329, *Space Sci. Instrum., 4*, 45, 1978.

Neubert, T., and K. J. Harker, Magnetic fields in the vicinity of pulsed electron beams in space., *Planet. Space Sci., 36*, 469, 1988.

Neubert, T., W. W. L. Taylor, L. R. O. Storey, N. Kawashima, W. T. Roberts, D. L. Reasoner, P. M. Banks, D. A. Gurnett, R. L. Williams, and J. Burch, Waves generated during electron beam emissions from the space shuttle, *J. Geophys. Res., 91*, 11321, 1986*a*.

Neubert, T., G. Holmgren, E. Ungstrup, and K. Melgard, Waves with harmonic structure below and above the lower hybrid resonance observed on the CENTAUR 35. 001 and 35. 002 rockets., *Can. J. Phys., 64*, 1437, 1986*b*.

Neubert, T., J. G. Hawkins, G. D. Reeves, P. M. Banks, R. I. Bush, P. R. Williamson, D. A. Gurnett, and W. J. Raitt, Pulsed

electron beam emissions in space, *J. Geomagn. Geoelectr.*, in press, 1988.

Obayashi, T., et al., Space experiments with particle accelerators (SEPAC), in *Artificial Particle Beams in Space Plasma Studies*, edited by B. Grandal, p. 659, Plenum, New York, 1982.

Reeves, G. D., Very low frequency radio waves produced by electron beam injection in space plasmas, Ph. D. dissertation, Stanford Univ., Stanford, Calif., 1988.

Reeves, G. D., P. M. Banks, A. C. Fraser-Smith, T. Neubert, R. I. Bush, D. A. Gurnett, and W. J. Raitt, VLF wave stimulation by pulsed electron beams injected from the space shuttle, *J. Geophys., Res., 93*, 162, 1988.

Sasaki, S., K.-I. Oyama, N. Kawashima, W. J. Raitt, and N. B. Myers, VLF and HF Wave characteristics observed from an active experiment tethered mother/daughter rocket payload (CHARGE-2), *EOS Trans. AGU*, 67, 1170, 1986*a*.

Sasaki, S., N. Kawashima, K. Kuriki, M. Yanagisawa, and T. Obayashi, Vehicle charging observed in SEPAC Spacelab 1 experiment, *J. Spacecr. Rockets, 23*, 194, 1986*b*.

Shawhan, S. D., G. B Murphy, and J. S. Pickett, Plasma diagnostics package initial assessment of the STS 3 orbiter plasma environment, *J. Spacecr. Rockets, 21*, 387, 1984*a*.

Shawhan, S. D., G. B. Murphy, P. M. Banks, P. R. Williamson, and W. J. Raitt, Wave emissions from dc and modulated electron beams on STS 3, *Radio Sci., 19*, 471, 1984*b*.

Tribble, A. C., N. D'Angelo, G. B. Murphy, J. S. Pickett, and J. T. Steinberg, Exposed high-voltage source effect on the potential of an ionospheric satellite, *J. Spacecr. Rockets*, in press, 1988.

Winckler, J. R., The application of artificial electron beams to magnetospheric research, *Rev. Geophys., 18*, 659, 1980.

Winckler, J. R., J. E. Steffen, P. R. Malcolm, K. N. Erickson, Y. Abe, and R. L. Swanson, Ion resonances and ELF wave production by an electron beam injected into the ionosphere: Echo 6, *J. Geophys. Res., 89*, 7565, 1984.

Winckler, J. R., K. E. Erickson, Y. Abe, J. E. Steffen, and P. R. Malcolm, ELF wave production by an electron beam emitting rocket system and its suppression on auroral field lines, *Geophys. Res. Lett., 12*, 457, 1985.

---

P. M. Banks, R. I. Bush, A. C. Fraser-Smith, T. Neubert, G. D. Reeves, and P. R. Williamson, STAR Laboratory, Durand 202, Stanford University, Stanford CA 94305.

D. A. Gurnett, Department of Physics and Astronomy, University of Iowa, Iowa City, IA 52242.

W. J. Raitt, Center for Atmospheric and Space Science, Utah State University, Logan, UT 84322

(received April 18, 1988;
revised July 13, 1988;
accepted August 29, 1988.)

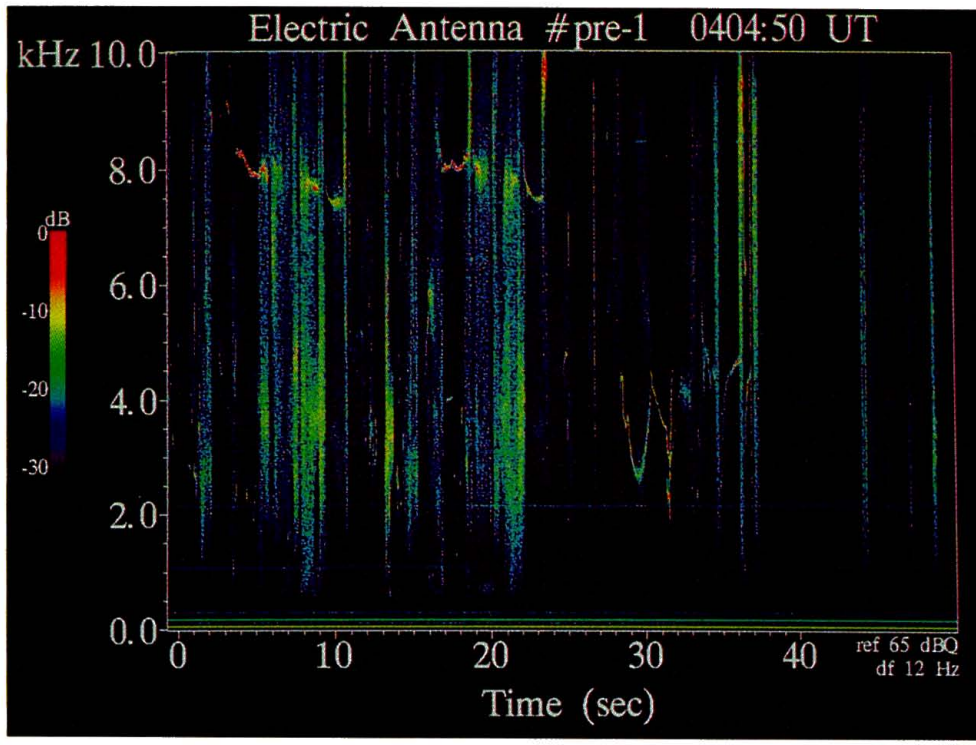


Plate 1*a* [*Reeves et al.*]. An antenna period from the Pulsed flux tube connection sequence before FPEG turn-on. The ambient wave field includes natural atmospherics, including whistlers; orbiter thruster-generated waves; and narrow-band, variable frequency emissions.

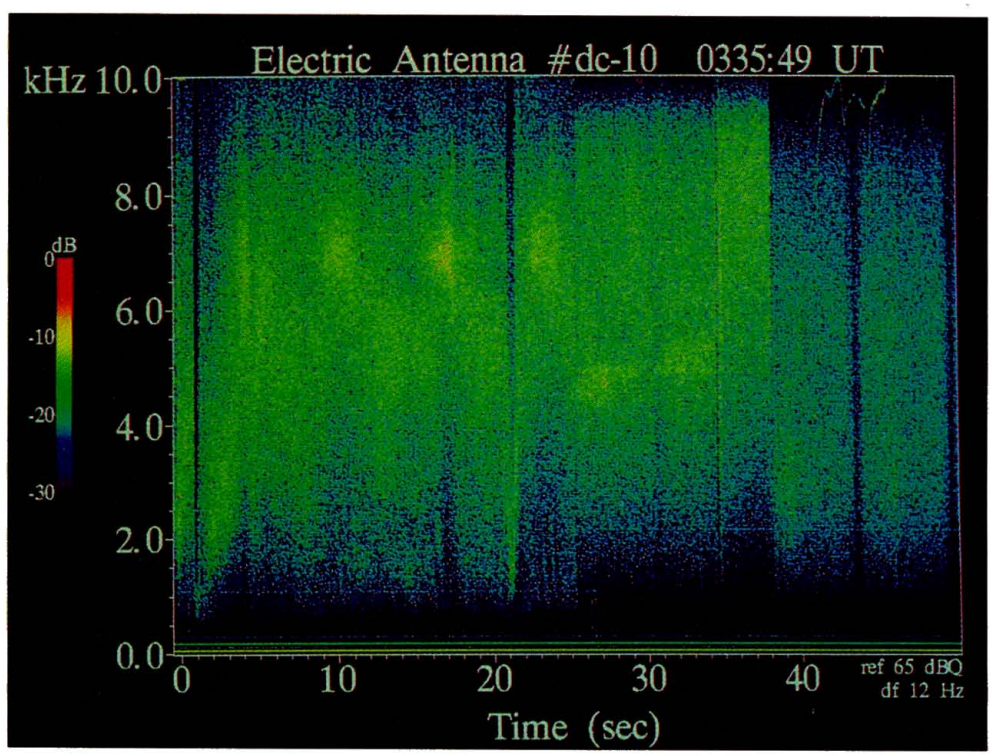


Plate 1*b* [*Reeves et al.*]. An antenna period from the DC flux tube connection sequence. The FPEG is operating in dc mode with a 50-mA beam current. Broadband beam-generated emissions are observed and the amplitude of these emissions is modulated by the spin of the PDP.

Plate 1 [*Reeves et al.*]. Spectrograms of four antenna periods during the Spacelab 2 mission. The antenna switching pattern is superimposed on the data so the first 26 s are 0–10 kHz, the next 13 s are 10–20 kHz (with 10 kHz at the top), and the final 13 s are 20–30 kHz. The AGC modulation of the amplitudes has not been removed, so amplitudes are relative.

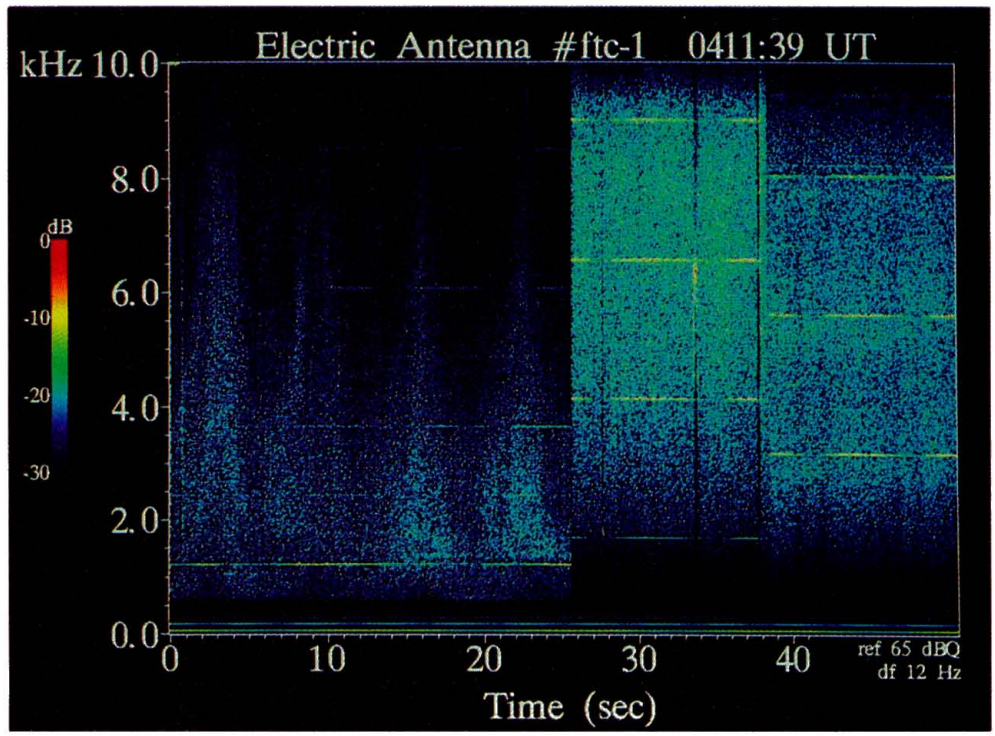


Plate 1*c* [*Reeves et al.*]. An antenna period from the Pulsed flux tube connection when the FPEG is pulsing with a 100-mA beam current and a 50% duty cycle at 1.22 kHz. Narrow-band harmonics and broadband emissions are observed and are spin modulated.

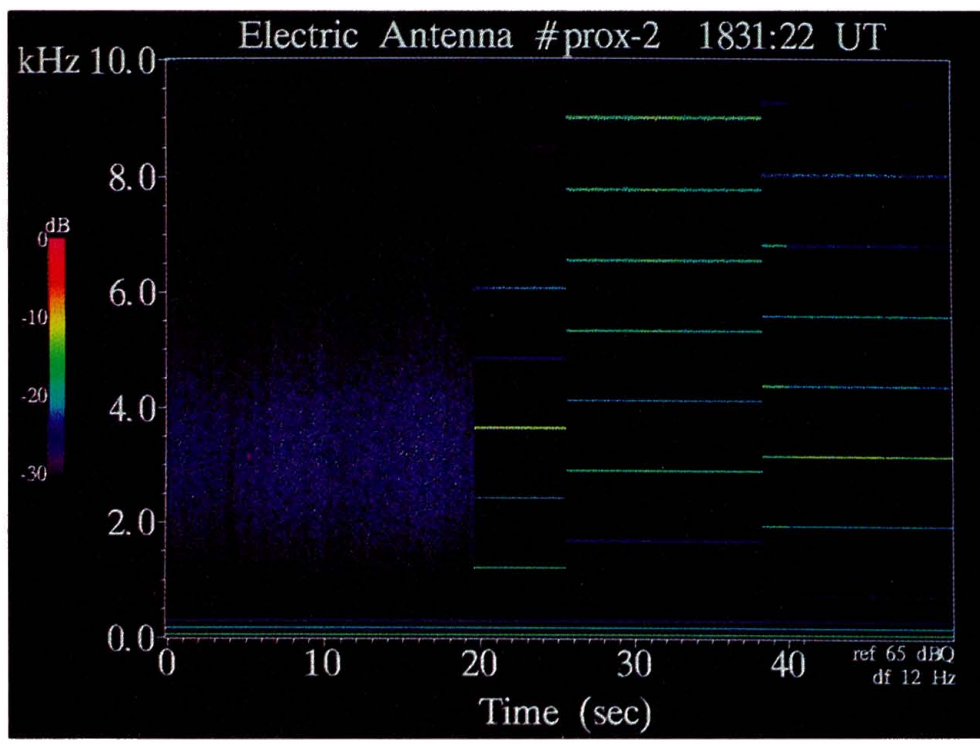


Plate 1*d* [*Reeves et al.*]. An antenna period from the Prox Ops sequence when the PDP is in the payload bay and the FPEG is pulsing at 1.22 kHz, 100-mA, 50% duty cycle. Strong narrow-band harmonics are seen beginning 19 s into the antenna period when the FPEG is turned on.